The transcriptional and epigenetic reprogramming mediated by chronic IL1β exposure drives self-renewal ability and myeloid priming in TET2 deficient stem and progenitor cells.

McClatchy J.[1,2*], Strogantsev R.[3*], Wolfe E. [1,2], Estabrook J.[3], Lin H.[1,2], Mohammadhosseini M.[1,2], Davis B.A. [1,2], Eden C.[1,2], Goldman D.[4,5], Fleming W.H.[4,5], Cimmino L.[6], Mohammed H.[3#], Agarwal A.[1,2,3,4,7#$]

[1]Division of Oncological Sciences, Oregon Health & Science University, Portland, OR, USA
[2]Department of Cell, Developmental, and Cancer Biology, Oregon Health & Science University, Portland, OR, USA
[3]Cancer Early Detection Advanced Research Center, Knight Cancer Institute, Oregon Health & Science University, Portland, OR, USA
[4]Division of Hematology & Medical Oncology, Oregon Health & Science University, Portland, OR, USA
[5]Division of Pediatric Hematology and Oncology, Oregon Health & Science University, Portland, OR, USA
[6]University of Miami, Miami, USA
[7]Department of Molecular and Medical Genetics, Oregon Health & Science University, Portland, OR, USA

*Co-first authors
#Co-senior authors

[§]Correspondence:

Anupriya Agarwal, PhD
Mail Code: KR-HEM | 3181 S.W. Sam Jackson Park Road | Portland OR 97239
Ph: 503-494-7599 email: agarwala@ohsu.edu

ABSTRACT

Clonal hematopoiesis (CH) increases risk for the development of hematological malignancy and cardiovascular disease. IL1β is elevated in patients with CH and its inhibition mitigates cardiovascular risk in murine models with *Tet2* loss-of-function. How IL1β alters population dynamics of hematopoietic cells upon *Tet2* deletion (*Tet2*-KO) is not well understood. We demonstrated IL1β expands *Tet2*-KO neutrophils, monocytes/macrophages, and long-term hematopoietic stem cells with reduced lymphopoiesis. IL1β promoted myeloid bias over other lineages of *Tet2*-KO HSPCs coinciding with failure to demethylate lineage associated enhancer and transcription factor binding sites. IL1β enhanced the self-renewal ability of *Tet2*-KO HSPCs by upregulating genes associated with self-renewal potential and by resisting demethylation of binding sites of transcription factors promoting terminal differentiation. IL1β-mediated premalignant phenotype is reversed by IL1β antagonist anakinra or deletion of the *Il1* receptor, *in vivo*. Our results demonstrated that targeting IL-1 signaling could be an efficient early intervention strategy in preleukemic disorders.

INTRODUCTION

Age related-clonal hematopoiesis (CH) occurs when a single hematopoietic stem/progenitor cell (HSPC) gains a selective advantage over other stem cells in bone marrow in the absence of hematological malignancy[1]. Approximately 10% of individuals over 60 years of age have CH with >2% variant allele frequency in the peripheral blood. CH is a potent risk factor for the development of cardiovascular disease, pulmonary disease, type 2 diabetes, and hematological malignancies[2-4]. Further, CH is associated with adverse outcomes even after onset of these malignancies[5]. Thus, understanding the mechanisms by which premalignant HSPCs gain a fitness advantage will assist in designing better strategies for disease monitoring, prevention, and surveillance.

TET2 loss-of-function mutations are one of the most common mutations in CH, present in approximately one third of cases[2]. *Tet2*-deficient murine HSPCs are shown to have increased self-renewal potential[6]. Studies have identified inflammatory cytokines, including IL1β, IL6, and TNFα, are elevated in individuals and murine models with TET2 CH. These studies suggest that inflammatory cytokines exert a selective pressure to drive aberrant myeloid expansion of preleukemic cells *in vivo*[7-9] in CH. Mechanistic work with IL6 has highlighted resistance to apoptosis as a driving factor in *Tet2*-KO HSPC expansion[7]. Further, TNFα favors in *vitro* expansion through a mechanism likely related to reduced apoptosis in *TET2* mutant HSPCs compared with wild-type cells[10]. Here, we focused on IL1β-modeled chronic inflammation, as targeting IL1β signaling is a promising cancer therapeutic[11,12,13] and improves outcomes of cardiac ischemia in murine models of CH[14]. To date a study integrating how long-term exposure to IL1β-driven inflammation alters the relative fitness of *TET2*-mutated HSPCs over healthy HSPCs remains elusive.

Using murine models with pan-hematopoietic specific *Tet2* deletion we showed these mice represent major features of *Tet2* myeloproliferation under IL1β-mediated chronic inflammatory stress. Specifically, we demonstrated that IL1β potentiated self-renewal ability of *Tet2*-KO HSPCs with increased myeloid bias and differentiation to pro-inflammatory monocytes/macrophages and neutrophils. These findings are mechanistically supported using single cell transcriptomic analysis and methylation profiling. Importantly, targeting IL1 signaling rescued aberrant myeloid expansion; thus, offering a preventative strategy for early intervention for individuals with CH.

RESULTS

IL1β exposure promotes neutrophilic and monocytic expansion of *Tet2*-KO cells over wild-type cells. IL1β is a potent pro-inflammatory cytokine elevated in human and murine *TET2* loss-of-function mutations-mediated CH[14-16]. To identify the impact of chronic IL1β exposure on the function and differentiation of HSPCs in TET2-mediated CH, we first used pan-hematopoietic *Tet2* loss-of-function mice (*Vav-Cre Tet2*$^{fl/fl}$, referred as *Tet2*-KO). We transplanted equal number of lineage negative progenitors derived from the bone marrow (BM) of *Tet2*-KO (CD45.2) and WT (CD45.1) mice into WT (CD45.1/45.2) recipients and treated daily with or without IL1β for 15 weeks (Supplementary Fig. 1a). Flow cytometric analysis of the peripheral blood (PB) was performed weekly. BM and spleen cells were analyzed at week five and fifteen. Treatment with IL1β increased frequency of *Tet2*-KO hematopoietic cells and CD11b^{+} myeloid cells in PB overtime (Supplementary Fig. 1b). Further, at week 15 IL1β promoted aberrant myeloid expansion of the *Tet2*-KO CD11b^{+}Gr1^{hi} (CD11b^{+}Ly6c^{hi}Ly6g^{hi}) subset[8] (Supplementary Fig. 1c). Notably, this increase occurred without change in the frequency of CD11b^{+}Gr1^{lo} (CD11b^{+}Ly6c^{lo}Ly6g^{lo} cells) in the PB or BM. Accordingly, CD11b^{+}Gr1^{hi} trended towards greater expansion than CD11b^{+}Gr1^{lo} in the spleen in *Tet2*-KO relative to WT mice treated with IL1β. Similar trends were observed within five weeks of treatment (Supplementary Fig. 1c). T cell frequency was reduced in *Tet2*-KO relative to WT in all conditions; however, B cell frequency reduction was IL1β dependent for the PB overtime as well as BM and spleen at week 15 (Supplementary Fig. 1d).

As different CD45 isoforms can alter differentiation and reconstitution[17] and lethal irradiation in recipient mice may cause alterations within the BM niche in transplantation experiments, we used *Tet2*-KO CD45.2 and WT CD45.2 (*Tet2*$^{fl/fl}$) treated with IL1β for five weeks to validate alterations in myeloid cell frequency (Fig. 1a). Weekly blood cell counts revealed *Tet2*-KO mice treated with

IL1β underwent a pronounced myeloid expansion overtime relative to WT mice treated with IL1β. In contrast, lymphocytes undergo a reduction in *Tet2*-KO relative to untreated controls with no alteration in erythrocytes or platelets (Supplementary Fig. 2a). *Tet2*-KO mice treated with IL1β developed splenomegaly, show increased frequency of myeloid cells in the PB overtime, as well as neutrophils and $CD11b^{+}Ly6c^{hi}Ly6g^{-}$ ($Ly6c^{hi}$) monocytes/macrophages in spleen and BM. Notably, this occurred without increase in the frequency of $CD11b^{+}Ly6c^{lo}Ly6g^{-}$ ($Ly6c^{lo}$) monocytes/macrophages (Fig. 1b-c and Supplementary Fig. 2b), as observed in our competition model (Supplementary Fig. 1c).

To model acquisition of somatic *TET2* mutations in hematopoietic cells, we also used ROSA26-M2rtTA mice, which expresses a doxycycline inducible shRNA targeting *Tet2* (*shTet2*). Lineage depleted *shTet2* BM cells were transplanted into WT CD45.1/45.2 recipients in competition with WT CD45.1 BM cells and treated with doxycycline and IL1β for 6 weeks (Fig. 1d). Doxycycline-induced knockdown of *Tet2* was monitored by GFP expression (Supplementary Fig. 2c)[18]. IL1β expanded *shTet2* myeloid cells in the PB (Fig. 1e). Consistent with our *Vav-Cre*$^{+}$*Tet2*$^{fl/fl}$ models, neutrophils and $ly6c^{hi}$ monocytes/macrophages were elevated in the spleen and BM of *shTet2* mice relative to WT mice treated with IL1β. Interestingly two-weeks withdrawal of doxycycline led to reversal of *shTet2* IL1β specific expansion of $ly6c^{hi}$ monocyte/macrophages and suppression of $ly6c^{lo}$ monocyte/macrophages whereas neutrophils did not reverse in the spleen and partially reversed in the BM (Fig. 1f, Supplementary Fig. 2d). Our findings suggest TET2 loss-of-function enhances both neutrophil and $ly6c^{hi}$ monocyte/macrophage production in response to pro-inflammatory stress at the expense of lymphopoiesis.

IL1β exposure selectively expands *Tet2*-KO HSPCs while promoting their myeloid bias. To determine whether chronic IL1β exposure impacts differentiation and expansion of *Tet2*-KO

HSPCs, we analyzed *Tet2*-KO non-transplantation and *shTet2* competitive transplantation models described in Figure 1. LT-HSCs (Lin^{-}c-Kit^{+}Sca-1^{+}Flk2^{-}CD48^{-}CD150^{+}) but not ST-HSCs (Lin^{-}c-Kit^{+}Sca-1^{+}Flk2^{-}CD48^{-}CD150^{-}) were elevated in frequency within the BM and spleen of *Tet2*-KO mice relative to WT upon IL1β stimulation (Fig. 2a, Supplementary Fig. 3a). Similarly, BM LT-HSCs exhibited a larger fold increase in frequency than ST-HSCs in *shTet2* mice relative to WT (Fig. 2b, Supplementary Fig. 3b).

Under steady state and upon IL1β stimulation, *Tet2*-KO mice trended towards increased frequency of myeloid-erythroid-megakaryocyte biased multipotent progenitor 2 (MPP2s; Lin^{-}c-Kit^{+}Sca-1^{+}Flk2^{-}CD48^{+}CD150^{+}) and myeloid biased MPP3s (Lin^{-}c-Kit^{+}Sca-1^{+}Flk2^{-}CD48^{+}CD150^{-}) relative to WT mice in the BM. In contrast, IL1β exposure reduced frequency of lymphoid biased MPP4s (Lin^{-}c-Kit^{+}Sca-1^{+}Flk2^{+}CD48^{+}CD150^{-}) in the BM of *Tet2*-KO mice relative to WT. Further, in the spleen, all MPP subsets were increased, but the magnitude of increase was smallest for MPP4s (Fig. 2c). Notably, MPP3s were elevated in *shTet2* mice relative to WT both with and without IL1β stimulation and this expansion was reversed upon doxycycline withdrawal. In contrast, MPP2 expansion is increased in *shTet2* mice in spleen and BM upon IL1β stimulation (Fig. 2d-e, Supplementary Fig. 3b). Further down the hematopoietic hierarchy, common myeloid progenitors (CMPs; Lin^{-}c-Kit^{+}Sca-1^{-}FCγRIII/II^{-}CD34^{+}) trended towards elevation in the spleen of *Tet2*-KO mice both with and without IL1β stimulation. Importantly, their differentiation at steady state and upon IL1β stimulation skewed towards granulocyte-monocyte progenitors (GMPs; Lin^{-}c-Kit^{+}Sca-1^{-}FCγRIII/II^{+}CD34^{+}) over megakaryocyte-erythrocyte progenitors (MEPs; Lin^{-}c-Kit^{+}Sca-1^{-}FCγRIII/II^{-}CD34^{-}) in BM and spleens of *Tet2*-KO mice relative to WT (Fig. 2f, Supplementary Fig. 4a). Cumulatively these data suggest IL1β stimulation promotes myeloid bias over lymphoid at the MPP stage of lineage commitment while myeloid bias over erythroid-

megakaryocytic occurs within CMPs for *Tet2*-KO mice (Fig. 2g). *TET2* deletion within HSPCs is essential for myeloid biasing, as myeloid lineage specific *LysM-Cre Tet2*$^{fl/fl}$ (*LysM-Cre Tet2*-KO) mice which exhibit *Tet2* deletion predominately in GMPs onwards[19] did not display expansion or myeloid bias in a competitive repopulation model over 18 weeks of exposure with IL1β stimulation relative to WT (Supplementary Fig. 4b).

Chronic IL1β exposure enhances the self-renewal capacity of *Tet2*-KO HSPCs driving their expansion. To assess how IL1β drives *Tet2*-KO HSPCs expansion, we used an *in vitro* competition assay, in which equal numbers of BM derived CD45.2 *Tet2*-KO and CD45.1 WT Lin$^-$Sca1$^+$cKit$^+$ (LSK) cells were cultured in competition with or without IL1β (Fig. 3a)[20]. Consistent with *in vivo* assays, IL1β stimulation of *Tet2*-KO LSKs enhanced expansion and myeloid bias overtime relative to WT LSKs (Supplementary Fig. 5a). *Tet2*-KO LSKs cultured with IL1β exhibited slower loss of Lin$^-$, LK, and LKS progenitors at week 1 relative to WT cells (Fig. 3a). We examined differences in the frequency of apoptosis as a potential driving factor and found IL1β did not exert significant effect on *Tet2*-KO HSPCs relative to WT *in vitro* (Supplementary Fig. 5b). To validate these findings *in vivo,* we treated WT and *Tet2*-KO mice with or without IL1β for 4 weeks. We observed only a mild trend towards reduction in frequency of apoptosis in HSPC subsets in *Tet2*-KO relative to WT mice (Supplementary Fig. 5c).

We next examined the impact of IL1β-mediated stress on cell cycle status of HSPCs *in vivo*. In steady state a significant portion of HSCs do not contribute to hematopoiesis and are largely quiescent, a mechanism to protect HSC function[21]. IL1β administration *in vivo* did not alter proportions of *Tet2*-KO LSKs in G_0. In contrast, WT LSKs underwent a reduction in frequency of G_0 cells. Interestingly, BM LSK cells in *Tet2*-KO mice showed increased S phase frequency upon

IL1β exposure compared to vehicle treated *Tet2*-KO cells, similar to WT, perhaps indicative that LSK cells in *Tet2*-KO mice are actively cycling while maintaining a G_0 pool (Fig. 3b). In contrast to LSKs, *Tet2*-KO LKs trended towards lower G_0 than WT LKs under IL1β stimulation, suggesting maintenance of G_0 pool is specific to LSK cells in *Tet2*-KO mice.

Given these findings and that *Tet2*-KO HSPCs are known to display increased self-renewal capacity at steady state[6,20], we tested whether IL1β stimulation cooperates with *TET2*-loss-of function to impact the self-renewal potential of HSPCs. Interestingly, upon IL1β stimulation *Tet2*-KO LSKs exhibited significantly enhanced self-renewal capacity relative to vehicle treated *Tet2*-KO cells in a serial re-plating assay with increased CFU-GMs or CFU-Ms up to the quaternary plating (Fig. 3c). In contrast, WT LSKs exhausted by the tertiary plating. Taken together, these studies suggest under prolonged IL1β induced inflammation, the primary fitness advantage of *Tet2*-KO HSPCs is mediated by increased self-renewal.

Single cell gene expression analysis reveals that *Tet2*-KO HSCs exhibit an enrichment of transcriptional signature associated with chronic stress and self-renewal capacity. To identify the mechanisms by which IL1β promotes myeloid expansion and self-renewal of *Tet2*-KO HSPCs, we performed single cell transcriptomic analysis of lineage depleted BM cells derived from *Tet2*-KO and WT mice treated with or without IL1β for 5 weeks (Fig. 4a). We identified 17 clusters both in WT and *Tet2*-KO mice (Supplementary Fig. 6a). Consistent with flow cytometry analysis *Tet2*-KO mice at steady state and upon IL-1β stimulation show expansion of HSCs and granulocyte/monocyte progenitors compared to respective wild-type controls (Fig. 4b). We focused on the HSC cluster and identified substantially more upregulated genes, 339 versus 41, in *Tet2*-KO mice relative to WT treated with IL1β with little change in the number of down regulated

genes (Fig. 4c,d). Enrichr and STRING analyses revealed enrichment for response to cytokines, stress, and reduced proliferation in *Tet2*-KO HSCs both at steady state and upon IL1β stimulation. Notably, *Tet2*-KO HSCs relative to WT enriched for transcriptional signatures of cancer, myelopoiesis, and dysregulation of lymphopoiesis and hematopoiesis upon IL1β stimulation but not in steady state (Supplementary Fig. 6b-c). Similar to gene ontology analyses, gene set enrichment analysis (GSEA) of *Tet2*-KO relative to WT HSCs at steady state and under IL1β stimulation identified enrichment of many inflammatory pathways including IFNα/β, TNFα, LPS regulated signaling as well as negative and positive mediators of MAPK signaling (Fig. 4e), suggesting *Tet2*-KO HSCs experience chronic inflammatory stress. To query whether IL1β stimulation elicits similar stress responses to aging, we used a published old HSCs gene signature[22]. This signature lay predominately within HSCs (Supplementary Fig. 6d), and was enriched in *Tet2*-KO relative to WT HSCs at steady state and upon IL1β stimulation (Fig. 4f). This signature includes phosphatases (*Ier2/5*, *Dusp1/2/5/6*) and transcription factors (*Egr1, AP-1* members: *Fos*, *Fosb, Jun, JunD*; kruppel-like factor members: *Klf2/4/6*) with roles in mediating and mitigating stress responses (Fig. 4d). Further, both at steady state and upon IL1β-mediated stress, several genes known to maintain HSC frequency under stress such as *Txnip* and *Kdm6b* were upregulated in *Tet2*-KO HSCs relative to WT [23,24] (Fig. 4d, Supplementary Fig. 6e). Cumulatively these results demonstrate *Tet2*-KO HSCs exhibit transcriptional signatures for chronic stress which can be magnified by inflammation such as IL1β. These findings also suggest *Tet2*-KO HSCs are adapted to better tolerate inflammatory stress, maintaining their HSC pool relative to WT.

Consistent with inflammation tolerance within *Tet2*-KO HSCs, GSEA identified significant enrichment of multiple pathways associated with self-renewal capacity in *Tet2*-KO HSCs relative

to WT upon IL1β stimulation, whereas only a single pathway was significant at steady state (Fig. 4e). *Tet2*-KO HSCs relative to WT HSCs upon IL1β stimulation showed an enrichment of HSC and leukemic stem cell signatures versus that of multipotent progenitor signatures. Specifically, we found significant upregulation of *Erg*, *Meis1,* and *Egr1* each associated with self-renewal ability[25-27] (Fig. 4d). Accordingly, proliferative signatures, which correspond to decreased self-renewal capacity, are downregulated in *Tet2*-KO HSCs relative to WT when treated with IL1β (Fig 4e)[20,28]. Cumulatively, these data suggest that *Tet2*-KO HSCs occupy a chronically stressed niche but display transcriptional programming that allows them to tolerate inflammatory insult by enhancing the transcription of self-renewal promoting genes.

IL1β promotes aberrant myeloid transcriptional priming of *Tet2*-KO HSCs.

Myeloid leukemia signatures are enriched in *Tet2*-KO HSCs relative to WT at steady state and upon IL1β stimulation (Fig. 4e). Accordingly, genes with roles in myeloid biasing, such as *Hmga2* was upregulated with and without IL1β stimulation while *Hlf* was upregulated upon IL1β stimulation alone in *Tet2*-KO HSCs relative to WT (Fig. 4d)[29,30]. Likewise, we identified upregulation in erythroid/megakaryocyte promoting pathways. In contrast pathways associated with lymphopoiesis were negatively enriched at steady state and upon IL1β stimulation, respectively (Fig. 4e). Accordingly, pseudotime analysis using single cell transcriptomic data revealed that *Tet2*-KO cells upon IL1β stimulation exhibits preferential commitment towards the myeloid biased granulocyte and monocyte progenitors but not towards erythroid or lymphoid lineages (Fig. 4g, Supplementary Fig. 7). Cumulatively, this supports that IL1β promotes aberrant myeloid differentiation transcriptional programs in *Tet2*-KO HSCs.

Hypermethylation of lineage specific enhancers and transcription factor binding sites coincides with cell fate of *Tet2*-KO HSPCs. To identify DNA methylation patterns specific to *Tet2*-KO HSPCs, we performed whole genome bisulfite sequencing (WGBS) using purified LSKs, CMPs, and GMPs derived from the BM of *Tet2*-KO and WT mice treated for 5 weeks with and without IL1β (Supplementary Fig. 8a). As expected *Tet2*-KO LSKs, CMPs, and GMPs exhibited higher global methylation and a greater number of hypermethylated differentially methylated regions (DMRs) than WT at steady state. These differences in hypermethylation between *Tet2*-KO and WT progenitors were exaggerated upon IL1β stimulation. This was largely resultant from the loss of global methylation in WT LSKs, CMPs, and GMPs upon IL1β treatment which was abrogated in *Tet2*-KO progenitors (Fig. 5a, Supplementary Fig. 8b). We found that DMRs in *Tet2*-KO LSKs, CMPs, and GMPs relative to WT were preferentially located in enhancer sites, with less within CpG islands as described previously[31-33]. Notably, *Tet2*-KO LSKs relative to WT upon IL1β stimulation had the highest percentage of their probes hypermethylated for lymphoid enhancers, followed by myeloid, and erythroid enhancers. In contrast, the opposite pattern was observed in *Tet2*-KO CMPs relative to WT upon IL1β stimulation in which erythroid enhancers were hypermethylated most (Fig 5b). This is consistent with our observation where upon IL1β stimulation, the differentiation of *Tet2*-KO HSPCs moved away from lymphoid-biased MPP4s and towards erythroid-myeloid biased MPP2s. Similarly, CMPs biased away from MEPs (Fig 2c-g) towards GMPs.

To further validate this finding, we used published ChIP-seq data for 35 proteins including transcription factors (TFs) and epigenetic modifiers with roles in maintenance of HSC function, differentiation, or inflammation. The top 10 TF binding sites with the highest methylation increase in *Tet2*-KO relative to WT upon IL1β stimulation in CMPs included

GATA1, TAL1, and MAZ which promote erythropoiesis (Fig 5c)[34-36]. The latter two binding sites were in the top 10 for methylation increase at steady state. Among these, overrepresentation of MAZ motif was identified within hypermethylated DMRs by HOMER analysis (Supplementary Figure 8c). In contrast, within LSKs many potent drivers of lymphopoiesis, including BACH2, BATF, ETS1, IKZF1, and RAG2 had binding sites which underwent pronounced hypermethylation in *Tet2*-KO relative to WT upon IL1β stimulation. HOMER analysis verified BACH2, BATF, and ETS1 were enriched in hypermethylated regions within LSKs but not in CMPs (Fig 5c, Supplementary Figure 8d). Cumulatively, these data suggest *Tet2*-KO HSCs lineage bias under inflammatory stress coincides with hypermethylation of different lineage promoting enhancer and transcription factor binding sites throughout hematopoiesis.

Further, TFs known to drive terminal hematopoietic differentiation (ELF4, PU.1, CEBPB, JUN)[37-40] are among the most methylated binding sites in *Tet2*-KO LSKs upon IL1β stimulation. In contrast, these same TFs within CMPs are below the average change in methylation between *Tet2*-KO and WT for all genomic probes (Fig. 5c). These factors binding motifs were confirmed by HOMER analysis to be over-represented within DMRs in *Tet2*-KO relative to WT LSKs upon IL1β stimulation. Notably, these same factors were not enriched within CMPs, suggesting specificity to the LSKs (Fig. 5d). Thus, abrogation of transcriptional programs promoting terminal differentiation by failure of TET2 to demethylate these binding sites may account for enhanced self-renewal capacity in *Tet2*-KO relative to WT under IL1β treatment.

We examined the top 150 downregulated genes from *Tet2*-KO HSCs relative to WT HSCs that are stimulated with IL1β identified using single cell RNAseq analysis (Fig 4). We found 38 genes proximal to hypermethylated binding sites of TFs (Fig. 5e). These include, promotor

hypermethylation corresponding with regulators of proliferation (*Cdk4*, *Mki67*). Intragenic methylation differences were also prominent in many TFs binding sites which promote proliferation (*mki67*, *Rrm1*, *Rrm2*, and *Cdk4*), which may account for reduced *Tet2*-KO HSCs proliferation in response to inflammatory signals, protecting their HSC pool (Supplementary Fig. 8e). Altogether, our data suggest that *Tet2*-KO HSCs lineage bias, self-renewal potential, and stem cell pool maintenance under inflammatory stress is mediated by epigenetic reprograming.

Antagonizing IL1β signaling abrogates aberrant myeloid expansion. To determine whether endogenous IL1β signaling plays a critical role in *Tet2*-mediated premalignant expansion, we bred *Tet2*-KO mice lacking interleukin 1 receptor 1 (*Il1r1)* referred as DKO (*Vav-cre Tet2*$^{fl/fl}$*Il1r1*)[41]. We examined the PB of *Tet2*-KO, WT, *Il1r1*-KO, and DKO mice older than 4 months, which is when myeloid expansion has been shown to occur previously (Fig. 6a)[42]. Differential blood cell counts revealed DKO mice were protected from skewed neutrophil production, monocytosis, and lymphopenia observed in *Tet2*-KO mice (Fig. 6b). These results are confirmed by flow cytometric analysis of PB (Supplementary Fig. 9a). Additionally, Ly6c^{hi} monocyte expansion was correlated positively with age in *Tet2*-KO mice but not in DKO (Fig. 6c). DKO mice relative to *Tet2*-KO trended towards higher RBC counts with no significant platelet abnormalities (Supplementary Fig. 9b). Cumulatively, these data support the role of endogenous IL1R1 signaling in *Tet2*-KO myeloid expansion.

We next examined whether treatment with an FDA approved IL1 receptor antagonist anakinra[43] (Ana) impedes *Tet2*-KO myeloid expansion in a competitive transplantation model (Fig. 6d). Mice treated with anakinra alone or in combination with IL1β over 5 weeks suppressed IL1β-mediated expansion of *Tet2*-KO cells in PB (Fig. 6e, Supplementary Fig 9c). Further, anakinra suppressed IL1β induced *Tet2-KO* myeloid expansion (Fig. 6f). Similarly, anakinra reduced IL1β induced

splenomegaly (Fig. 6g). Of note, upon anakinra treatment *Tet2*-KO LSK frequency trended towards a reduction in spleen with and without IL1β stimulation, returning to the baseline observed in WT mice (Supplementary Fig. 9d).

Finally, we performed CRISPR-Cas9 editing of *TET2* using human BM progenitors. We noticed increased colony formation, primarily constituted CFU-M, with *TET2*-edited progenitors upon IL1β stimulation but not with non-targeting controls. This effect on *TET2*-edited progenitors is reversed by IL1 receptor antagonist (IL1RA) (Fig 6h, Supplementary Fig. 9e). These data support the efficacy of IL1 receptor blockade in abrogating IL1β-mediated expansion of *TET2*-mutated human HSPCs and myeloid cells.

DISCUSSION

Inflammation is widely implicated in promoting expansion of TET2-mediated clonal hematopoiesis and associated myeloid bias[7-10]; however, the mechanism is not completely defined. We used multiple murine models of *TET2* loss-of-function to delineate the impact of IL1β-mediated inflammatory stress on hematopoiesis.

We showed exogenous IL1β drives expansion of *Tet2*-KO HSCs *in vitro* and *in vivo*. Mechanistically, we found no significant differences in apoptosis between *Tet2*-KO and WT HSPCs upon IL1β stimulation, whereas reductions in apoptosis of *Tet2*-KO HSPCs have been shown upon chronic exposure to TNFα or acute exposure to IL6[7,10]. This suggests various cytokines may differ in the mechanism by which they promote expansion of *TET2*-mutated cells. We observed elevated self-renewal capacity of *Tet2*-KO at steady state, as shown previously[6,18]. Importantly, IL1β substantially increased the self-renewal capacity of *Tet2*-KO LSKs, while WT HSPCs exhausted upon IL1β-mediated stress[20]. Accordingly, we observed upregulation of transcriptional signatures associated with self-renewal potential in *Tet2*-KO HSCs predominately under IL1β stimulation. HSCs begin active proliferation upon inflammatory insult, such as IFNα, LPS, and IL1β, which impairs their self-renewal capacity[20,28]. WT LSK cells reduced their frequency of G_0 cells upon IL1β stimulation, but *Tet2*-KO LSKs did not. Proliferative transcriptomic signatures are also downregulated in *Tet2*-KO relative to WT HSCs. Notably, the binding sites of TFs known to drive HSCs towards terminal differentiation (PU.1, ELF4, JUN) were hypermethylated in steady state in *Tet2*-KO relative to WT LSKs, which is further increased in magnitude upon IL1β stimulation. Similarly, IL1β promoted hypermethylation CEBPB binding sites, known to drive HSCs towards terminal differentiation, and promoted hypermethylation in genes driving proliferation, such as *Cdk4*[37-40].

Further, in *Tet2*-KO HSCs relative to WT, we found strong enrichment of the transcriptional signature specific to old HSCs[22] as well as upregulation of AP-1 members (*Jun*, *Jund Fos*, *Fosb*) both in steady state and upon IL1β stimulation. However, *Tet2*-KO HSCs exhibited several putative mechanisms that may allow them to tolerate this continual stress. Predominately under IL1β stimulation, negative regulators of AP-1 (*Dusp1/2/5/6*) and NF- κB signaling (*Nfkbia*) are upregulated[44,45]. Further, there is hypermethylation of JUN binding sites in *Tet2*-KO LSK cells relative to WT in steady state which is enhanced by IL1β stimulation. These changes were specific to LSKs and not observed in CMPs or GMPs. Cumulatively these data suggest *Tet2*-KO HSPCs perpetuate and tolerate a chronically inflamed microenvironment due to both transcriptomic and epigenetic reprograming.

IL1β also drives myeloid expansion of *Tet2*-KO HSCs with myeloid bias over lymphoid lineage at the MPP stage where the first trifurcation of cell fate occurs. MPP3s frequency was elevated in steady state and upon IL1β stimulation whereas MPP2 frequency was elevated only upon IL1β stimulation. Accordingly, *Tet2*-KO relative to WT LSKs exhibited hypermethylation of lymphoid lineage promoting TFs binding sites at steady state which is enhanced by IL1β. This resulted from *Tet2*-KO resisting IL1β induced demethylation of lymphoid TFs binding sites observed in WT LSK cells. In contrast, hypermethylation of erythroid TFs binding sites and enhancers was elevated specifically within CMPs. After CMP bifurcation, there were increased GMPs over MEPs at steady state and upon IL1β stimulation in *Tet2*-KO relative to WT. This is consistent with previous findings of transcriptional priming towards myeloid lineage with erythroid suppression at steady state[31]. Cumulatively these data suggest inflammation exaggerates differential methylation of enhancers and lineage specific TF binding sites, coinciding with cell fate decisions favoring myeloid bias upon *TET2*- loss-of-function.

IL1β elevates the frequency of neutrophils and ly6c^{hi} monocytes/macrophages in *Tet2*-KO relative to WT. Previous studies show that Gr1 (ly6c/ly6g) positive cells expand in *Tet2*-KO PB[8], spleen[6] and BM[42] upon inflammatory stress or aging. This expansion is defined as aberrant *Tet2*-KO myelopoiesis in response to inflammation[7,8,18,46]. Pro-inflammatory monocytes/macrophages have significant roles in cardiovascular disease[47] and are elevated in murine *Tet2*-KO models[4] exhibiting poorer cardiovascular outcomes. Cardiovascular outcomes in these models are improved by IL1β inhibition[14]. Our findings show ly6c^{hi} monocytes/macrophages expansion is correlated with aging in *Tet2*-KO mice. This expansion is IL1 dependent in aging mice or rapidly abrogated by restoration of *Tet2* expression in a *Tet2*-shRNA model. Further, treatment with anakinra, a clinically approved IL1 receptor antagonist, reduced myeloid biasing of *Tet2*-KO cells. Notably, *TET2*-edited human progenitors produced increased monocyte colonies upon IL1β stimulation, which is blocked by an IL1 antagonist. IL1 signaling blockade is a promising therapeutic approach to treat inflammatory diseases[43], cancer[11,12,13,48], and cardiovascular diseases[49]. Cumulatively, our work highlights the therapeutic potential of inhibiting IL1β signaling for the treatment of CHIP associated premalignant myeloid expansion.

Online METHODS

Transgenic animals

A breeding colony of *Vav-Cre-Tet2*$^{fl/fl}$, described previously[6], were generously provided by Dr. Ross L. Levine from the Memorial Sloan Kettering Cancer Center, New York. Similarly, a breeding colony of *LysM-Cre-Tet2* $^{fl/fl}$ mice was generously provided by Dr. Evan Lind from Oregon Health and Science University (OHSU), Portland who acquired them from Jackson Laboratory (B6;129S-*Tet2*$^{tm1.1Iaai}$/J, Strain # 017573). ROSA26-M2rtTA (RTA) tetracycline-on *shTet2* mice, described previously[18], were provided by Dr. Luisa Cimmino, from New York University, New York. CD45.2^{+} (C57BL/6J, Strain # 000664), CD45.1^{+} (B6.SJL-*Ptprc*^{a} *Pepc*^{b}/BoyJ, Strain # 0002014), *Il1r1*-KO (B6.129S7-*Il1r1*^{tm1Imx}/J) mice strains were obtained from Jackson laboratory. Heterozygous CD45.1/45.2 mice were obtained by breeding CD45.1 and CD45.2 mice. Double Knockout mice (DKO) were obtained by breeding *Il1r1*-KO mice with *Vav-Cre-Tet2*$^{fl/fl}$. All mice were bred and maintained in the Department of Comparative Medicine at Oregon Health & Science University. All animal procedures were conducted in accordance with the Guidelines for the Care and Use of Laboratory Animals and were approved by the Institutional Animal Care and Use Committee.

Mouse genotyping

In house genotyping: Tails were clipped from 3-4 weeks old mice and lysed in 100 µL buffer (2 M Tris, pH 8.8; 1M ammonium sulfate; 0.5 M $MgCl_2$; 0.5% gelatin; deionized water; 2-ME; Triton X-100) containing proteinase K overnight at 55°C. DNA was diluted to 500 µL water and 2 µl was used for PCR analysis. Primers and PCRs were done as specified by protocols by Jackson

Laboratory. Identification of intact *Tet2* (Protocol 19042: Standard PCR Assay - Tet2<tm1.1Iaai> Version 2.0)

Tet2 Forward: AAG AAT TGC TAC AGG CCT GC

Tet2 Reverse: TTC TTT AGC CCT TGC TGA GC

Identification of excision of *Tet2*

Tet2 Forward: AAG AAT TGC TAC AGG CCT GC

Tet2 loxp3 Reverse: TAG AGG GAG GGG GCA TAA GT

For identification of *Lys-Cre* (Protocol 26499: Separated MCA Assay - Lyz2<tm1(cre)Ifo> Version 5.2)

Lys mutant: CCC AGA AAT GCC AGA TTA CG

Lys common: CTT GGG CTG CCA GAA TTT CTC

Lys wild type: TTA CAG TCG GCC AGG CTG AC

Identification of *Cre* expression (Protocol 27862: Standard PCR Assay - Generic cre 2 Version 3.2)

Cre control Forward: CTA GGC CAC AGA ATT GAA AGA TCT

Cre control Reverse: GTA GGT GGA AAT TCT AGC ATC ATC C

Cre trans Forward: AGA TGC CAG GAC ATC AGG AAC CTG

Cre trans Reverse: ATC AGC CAC ACC AGA CAC AGA GAT C

Vav-Cre-Tet2-KO, DKO, and *Il1r1*-KO genotyping was performed by Transnetyx with the following primers:

Tet2^{fl}

Forward Primer: CGGACGCCTCGTCAACA

Reverse Primer: GCTGGATCGGCTCTCTTATCTCATA

Tet2^{+}

Forward Primer: GGAGGTAGCCTTGAAGAACTTGAG

Reverse Primer: GCTGGATCGGCTCTCTTATCTCATA

Tet2^{-}

Forward Primer: CTTAAGTGTACACGCGTACTAGTCT

Reverse Primer: CAAGACCTCCCTGATGCTATGG

iCre

Forward Primer: TCCTGGGCATTGCCTACAAC

Reverse Primer: CTTCACTCTGATTCTGGCAATTTCG

Il1r1^{+}

Forward Primer: CACGGCGACACCATAATTTGG

Reverse Primer: GTCCCGGTCCGCTGATATG

Il1r1^{-}

Forward Primer: GCCTTCTTGACGAGTTCTTCTGA

Reverse Primer: CAAGAGCCATGCATGCTATTAATCC

Bone marrow transplantation

BM transplantation was performed as described previously[13]. Briefly, bones (femurs, tibias, and hipbones) of 6 to 8 weeks old mice were flushed with DMEM containing 10% FBS to isolate marrow. Bone marrow cells were incubated with ammonium chloride solution (Stemcells Tech, Vancouver, British Columbia, Canada) for red blood cells lysis. Lineage negative cells were

magnetically enriched using a lineage cell depletion kit (Miltenyl Biotec, San Jose, California) and incubated at 37^0C overnight in prestimulation media (DMEM supplemented with 1% Pen/Strep, 1X L-glutamine, 15% FBS, 15% WEHI-3B, mIL-3 7ng/mL, mIL-6 12ng/mL, mSCF 56 ng/mL). 2.5-5x10^5 lineage depleted cells were transplanted by retroorbital injection into lethally irradiated C57BL/6J recipients (500 cGy, 2 doses 4 hours apart). For *Vav-Cre Tet2*$^{fl/fl}$ and *Lys-Cre Tet2*$^{fl/fl}$ competition experiments donor mice were treated with 5-fluorouracil (5-FU) 100 mg/kg retro-orbitally. Non-transplant *Vav-Cre Tet2*$^{fl/fl}$ and sh*Tet2* competition experiments were performed without 5-FU administration. Three weeks after transplantation mice were treated with 500 ng/mouse/day of recombinant IL1β (Peprotech, Cranbury, New Jersey) intraperitoneally. For shTET2 competition experiment doxycycline was administered orally at 1mg/mouse. For *Vav-Cre Tet2*$^{fl/fl}$ competition experiments treated with IL-1β and/or anakinra, anakinra was administered daily subcutaneously (100mg/kg) 45 mins prior to the IL-1β treatments.

Differential blood counts

Weekly, 15 µl of blood collected from the saphenous vein was mixed with equal part 2mM EDTA and analyzed using a Vet ABC blood analyzer (Scil Animal Care Company, Barrie, Ontario, Canada) or the Element HT5 (Heska, Loveland, Colorado) according to manufacturer's directives.

Flow cytometry analysis

BM, spleen, and PB sample collection and staining were performed as described previously[13]. Briefly, BM cells were isolated from each animal by flushing the bones with DMEM containing 10% FBS. Red blood cells were lysed using aqueous solution of ammonium chloride (Stemcell

Tech., Vancouver, Canada). All staining for flow cytometry analysis involved Fc blocking with 2.5% by volume of heat shocked mouse serum for 10 minutes prior to staining and Fc blocking was maintained during staining. The data was collected using the Aria III cell sorter, BD LSRFortessa and the BD Symphony A5. The data was analyzed using FlowJo software. Gating for HSPCs[20] and differentiated markers was performed as described previously[7,8].

Weekly PB: Weekly PB samples were stained using PE-conjugated CD45.2, PE-Cy7-conjugated CD3, APC-conjugated CD11b and APC-Cy7-conjugated CD19 antibodies. For competition studies cells were distinguished by CD45 isoforms using the addition of PE-CF594-conjugated CD45.1.

Vav-cre Tet2$^{fl/fl}$ murine model competition experiments: An initial cocktail combined the weekly PB cocktail described above on ~10^5 cells isolated from the BM, spleen, and PB samples with the addition PerCP-Cy5.5-conjugated Gr1 to help visualize terminally differentiated populations. A second cocktail was used on BM and spleen cells to identify HSPCs. This cocktail was comprised of FVS510-conjugated Fixable Viability Stain, PE-CF594-conjugated CD45.1, PE-conjugated CD45.2, PercP-eFluor710-conjugated CD135, Alexa 700-conjugated CD34, APC-eFluor780-conjugated cKit, PE-Cy7-conjugated CD150, Pacific Blue-conjugated Sca1, and BV605-conjugated Fc Gamma (CD16/CD32) antibodies and lineage markers (CD3, CD4, CD8, B220, Gr-1, Ter-119, CD19, IgM, and CD127 all conjugated to APC).

For non-transplantation murine model experiments: An initial cocktail combined the weekly PB cocktail described above with the addition of BV650-conjugated Ly-6G and BV711-conjugated Ly-6C. A second cocktail identified apoptosis and cell death within HSPCs. This cocktail was

comprised of 7AAD, Annexin V, PE-conjugated Sca1, PercP-eFluor710-conjugated CD135, APC-conjugated lineage cocktail (described above), Alexa 700-conjugated CD34, APC-eFluor780-conjugated cKit, PE-Cy7-conjugated CD150, BV605-conjugated Fc Gamma (CD16/CD32) and BV711-conjugated CD48 antibodies. A third cocktail identified cell cycle by performing surface staining of PE-conjugated Sca1, APC-conjugated lineage cocktail (described above), Alexa 700-conjugated CD34, APC-eFluor780-conjugated cKit and BV605-conjugated Fc Gamma (CD16/CD32) for 30 minutes followed by fixation and permeabilization using BD Cytofix/Cytoperm (BD Biosciences, San Jose, California). Intracellular staining using FITC-conjugated KI-67 was performed overnight at 4 degrees, followed by staining with DAPI at with a final concentration of 0.5ug/ml.

Rosa shTET2 Transplantation experiments: The same staining cocktails were used as the non-transplantation model, with the following exception. GFP co-expressed with shRNA targeting *Tet2* was analyzed. PE-conjugated CD45.2 and PE-CF594-conjugated CD45.1 delineated CD45 isoforms. Pacific Blue-conjugated Sca1 was used in place of PE conjugated Sca1.

***In Vitro* competition assays**

In Vitro Competition: The assay was adopted from a previously published study (ref). BM was isolated as described previously from *Vav-Cre Tet2*$^{fl/fl}$ *(Tet2*-KO , CD45.2^{+}) and WT CD45.1^{+} mice and lineage depleted using the direct lineage cell depletion kit (Miltenyl Biotec, San Jose, California) according to manufacturer's instructions[13]. Cells were kept overnight in DMEM media containing 15% fetal bovine serum, 1% pen-strep, 2% L-Glutamine, 15% WEHI, mIL-3 (7 ng/mL), mIL-6 (12 ng/mL), and mSCF (56 ng/mL). Cells were stained with PE-conjugated Sca1,

APC-conjugated lineage cocktail, FITC-conjugated CD45.2, PE-CF594-conjugated CD45.1, APC-eFluor780-conjugated cKit and 7AAD and sorted by flow using the ARIA III at a density of 250 WT and 250 *Tet2*-KO $Lin^{-}Sca1^{+}cKit^{+}7AAD^{-}$ cells per well into a 96 well plate containing 200 µl of IMDM medium supplemented with 20% FBS, 100 ng/ml mSCF, 20 ng/mL mIL-3, 50 ng/mL mFlt-3L, 1% Pen/Strep with or without 25ng/mL of mIL1β. To feed cells, 50% of supernatant volume was removed carefully after cells had settled and replaced every 2-3 days. Every 3-4 days half the cells were analyzed by flow cytometry using PE-conjugated Sca1, FITC-conjugated CD45.2, PE-CF594-conjugated CD45.1, APC-conjugated lineage cocktail, AF700-conjugated CD11b, APC-eFluor780-conjugated cKit. Cells were counted on the same day as flow cytometric analysis by a Guava EasyCyte HT.

Apoptosis/Cell Death: For *in vitro* apoptosis studies cells were prepared as specified above, except 5000 WT and 5000 *Tet2*-KO cells were plated per well. The following day, cells were stained with annexin V, with PE-conjugated Sca1, FITC-conjugated CD45.2, PE-CF594-conjugated CD45.1, APC-conjugated lineage cocktail, APC-eFluor780-conjugated cKit and analyzed by flow cytometry.

Murine colony formation assay

BM cells were harvested from wild type and *Tet2*-KO mice (N=4, 8-12 weeks old). Cells were subjected to red cell lysis in 5 ml ammonium chloride lysis buffer solution (Stem Cell Technologies) on ice for 10 minutes. Lineage cells were depleted as described above. Cells were kept overnight in DMEM media containing 15% fetal bovine serum, 1% pen-strep, 2% L-Glutamine, 15% WEHI, mIL-3 (7 ng/mL), mIL-6 (12 ng/mL), and mSCF (56 ng/mL). Cells were

stained with PE-conjugated Sca1, APC-conjugated lineage cocktail, APC-eFluor780-conjugated cKit and 7AAD and purified by fluorescent activated cell sorting (FACS) at a density of 600 Lin^- $Sca1^+cKit^+7AAD^-$ cells per 1.1 ml/well of MethoCult™ M3334 (STEMCELL Technologies, Vancouver, British Columbia, Canada). M3334 methocult was supplemented with cytokines to a final concentration of 5 ng/ml mIL-3, 25 ng/mL mSCF, and with or without 25ng/ml mIL1β. Colonies were counted one week after plating and categorized as colony formation units (CFUs); CFU-G, CFU-M, CFU-GM or CFU-E. Cells from the colony formation assay were then resuspended in IMDM 2% FBS and re-plated at 1.2 x 10^5 cells/well in identical conditions up to the quaternary plating.

CRISPR-editing for *TET2* using human $CD34^+$ cells and colony formation assay

Healthy donor bone marrow was purchased commercially (Lonza inc). $CD34^+$ progenitor cells were enriched using magnetic CD34 microbead kit (Miltenyl Biotec, San Jose, California) and expanded overnight in SFEMII (Stem Cell Technologies) supplemented with SCF (100 ng/mL), TPO (100 ng/mL), FLT3-ligand (100 ng/mL), IL-6 (100 ng/mL), LDL (10 ug/mL), and UM171 (38 nM) (Peprotech, Cranbury, New Jersey). Cells were resuspended in Amaxa P3 Primary Cell solutions, and added to RNP complexes consisting of either a non-targeting scrambled sgRNA (Negative Control sgRNA (mod) #1; Synthego) or the multi-guide sgRNA (G1: AGAGCUCAUCCAGAAGUAAA; G2: UUAUGGAAUACCCUGUAUGA; G3: UCCUCCAUUUUGCAAACACU) provided with the Gene Knockout Kit v2 for human TET2 (Synthego, Redwood City, California). Cells were nucleofected with the program DZ-100 with a Lonza 4-D Nucleofector, and then immediately transferred to SFEMII. 24 hrs after nucleofection editing efficiency was quantified and we achieved an initial indel frequency of ~16%. For this

PCR was performed following primers: 5'-TCAACTAGAGGGCAGCCTTG-3' (F) and 5'-TGGCTTACCCCGAAGTTACG-3' (R), and conditions: 97°C for 5 min, then 35 cycles of 92°C for 30s, 60°C for 30s, 72°C for 20s, and a final extension at 72°C for 10 minutes. Sanger sequencing of PCR product was performed using forward primer and subsequently analyzed using Synthego ICE analysis tool. 24 hrs after nucleofection, cells were also plated at 600 cells per well in H4434 methocult with or without 25ng/ml hIL1β. Colonies were counted two weeks after plating and categorized as colony formation units (CFUs); CFU-G, CFU-M, CFU-GM or CFU-E. Individual colonies were picked, PCR amplified and sanger sequenced to determine indel frequency as described above.

Single cell RNA sequencing

BM cells were isolated from *Vav-Cre Tet2*$^{fl/fl}$*Tet2* KO and *Tet2*$^{fl/fl}$ (WT) mice treated with IL1β or vehicle for 5 weeks (N=4 per each genotype/condition, 8-12 weeks old) and lineage depleted using direct lineage cell depletion kit (Miltenyl Biotec, San Jose, California). The cells from each mouse were stained with TotalSeq^{TM} (Biolegend) cell hashing antibodies (Hash Tag 1: ACCCACCAGTAAGAC and Hash Tag 2: GGTCGAGAGCATTC) and washed. Two samples were mixed in equal proportions from two mice of the same genotype and treatment type, 8 sample pools total (16 samples). Each sample pool was loaded onto Chromium Controller (10x Genomics) to form single cell gel bead emulsions (GEMs) and reverse transcribed generating barcoded cDNA. Transcriptome (RNA) and hashtag (HTO) libraries were size selected using SPRI-beads and sequenced separately on a NovaSeq-6000 instrument.

Single cell RNA-seq Data analysis

A total of 54,984 barcoded single cell libraries were generated from the 10x scRNA-seq experiment. Cell Ranger package (10x Genomics) was used to align mRNA reads from 10x scRNA-seq libraries to murine GRCm38 (mm10) genome and generate feature-barcode matrices. Downstream analysis was performed using Seurat (v3) package with a set of standard vignettes[50]. Cells with n feature counts <750 and mitochondrial DNA content >10% were removed as low quality/ apoptotic cells. HTO libraries from hashtag antibody cell labeling were used to assign each cell to individual mice. Cells labelling with two HTO barcodes were excluded as potential doublets.

Dataset integration was performed using reciprocal PCA method with *Tet2* WT (vehicle treated) as a reference. Dimensionality reduction and clustering revealed 22 transcriptional clusters. Cell type assignment to each cluster was performed based on top marker expression per cluster and comparison to haemopedia RNA-seq reference[51]. These were then further cross-checked against known genes associated with specific lineages and cell types leading to 17 clusters[31,52,53]. Differentially expressed genes were identified between *Tet2* KO and WT as well as vehicle vs. IL1β treatment were identified for each cell type using 'FindMarkers' function in Seurat. DESeq2 analysis was performed to verify significant genes considering replicate samples.

Pseudotime analysis

Monocle3 v1.0.0 was used to calculate pseudotime values. The cells were clustered using the default parameters for the cluster_cell function based on the UMAP coordinates calculated with Seurat. The trajectory graph was built using the learn_graph function with the default parameters.

Diffusion pseudotime values were calculated using the order_cell function by programmatically selecting a node within the HSC cluster, identified through Seurat analysis, that is most heavily occupied by cells that have the earliest time point.

DNA methylation library preparation

Whole genome bisulfite sequencing (WGBS) libraries were prepared from FACS purified populations of LSK, CMP, and GMP cells using an ultra-sensitive method developed for single cell sequencing scBS-seq[54] and G&T-seq[55]. Briefly, ~500 flow sorted cells were resuspended in 2.5 µl of RLT plus buffer (Qiagen). Polyadenylated RNA was captured with oligo-dT conjugated beads and processed using Smart-seq2 protocol[56]. Remaining genomic DNA was bisulfite converted (EZ DNA methylation kit, Zymo) and the protocol for single cell BS-seq library preparation was followed[54]. A total of 48 libraries were prepared (N=4 animals per genotype/treatment, 3 cell types, *Tet2* WT/KO +/-IL1β), pooled using appropriate Illumina Truseq CD i5/i7 index adapters and sequenced on a Novaseq-6000 instrument (Illumina) to the depth of ~20x for LSK and ~4x for CMP and GMP samples.

DNA methylation analysis

Bisulfite sequencing (BS-seq) libraries were demultiplexed by the sequencing facility and processed on a slurm compute cluster aligning to GRCm38 murine genome. Detailed description of the alignment pipeline is described elsewhere[57]. Briefly, adaptor trimming was performed using trim_galore with following options: trim_galore –gzip –clip_r1 6 –clip_r2 6 –paired –fastqc

Genomic alignment were performed using bismark[58] aligner in a non-strand specific manner separately for read one and two:

bismark --non_directional --gzip -N 1 --parallel 4 --unmapped --score_min L,-10,-0.2

DNA methylation calls were extracted from the aligned reads as CpG coverage files and analyzed using the SeqMonk application. Differentially Methylated regions were defined in SeqMonk using windowed probes tiling 50 CpGs sites across the mouse genome. Probes with ≥10 CpGs with at least one read were quantified for average DNA methylation level using a SeqMonk in-built bisulfite sequencing quantitation pipeline. Logistic regression model was applied to define DMRs between *Tet2* WT vs KO cells with both vehicle or IL1β treatment conditions. Probes with p-value < 0.05 and absolute DNA methylation difference ≥10% were called as biologically significant.

Enhancer elements for different blood lineages were defined based on publicly available reference histone modification datasets[59]. Briefly, raw data was downloaded from the GEO database (GSE59636) and re-aligned to GRCm38 (mm10) murine genome. Enhancers for HSC, CMP, GMP, and MEP cells were defined as follows: first, H3K27ac peaks were called using Model-based analysis of ChIP-seq (MACS)[60] within the SeqMonk analysis tool. Second, H3K27ac peaks that did not overlap known promoter elements and had a higher H3K4me1 /H3K4me3 ratio were called as enhancers for each cell type. The CpG methylation of probes overlapping with an enhancer site for one and only one cell state (MEP, CMPs, GMPs, CLPs) were defined as specific probes and the rest were excluded.

DNA binding proteins constituting transcription factors and epigenetic regulators with known roles in hematopoiesis were chosen and supplemented with HOMER identified transcription factors with literature derived significance. These were limited to those with publicly available ChIP-seq binding data within embryonic stem cells or hematopoietic lineages (44 proteins). ChIP-seq "BED" files of called peaks were downloaded from Cistrome. When necessary, MGSCv37 (mm9) genome alignment was lifted to GRCm38 via UCSC "LiftOver". SeqMonk performed quantitation

of CpG methylation across defined probes spanning all DNA binding protein called peaks (784,110 probes). Of the 44 proteins chosen for ChIP-seq, 8 were excluded because they lacked sufficient probes with coverage (>100 probes) for at least one of the 48 samples, leaving 36 remaining factors. The difference in CpG methylation between each individual probe between *Tet2*-KO and WT was calculated. Values were referenced against the average difference between all CpGs with sufficient coverage for LSKs, CMPs and GMPs to identify transcription factors which possessed unusually high methylation.

To identify specific factors binding sites which may exhibit altered transcription due to methylation, ChIP binding sites of the 36 remaining factors were annotated by SeqMonk to determine genes within 2k base pairs with significant ($p < 0.05$) methylation changes. These genes were compared with the top 100 most significantly downregulated genes in *Tet2*-KO relative to WT. These genes were then manually annotated for function by literature search.

Gene set enrichment analysis

Gene set enrichment analysis pre-ranked was performed using the GSEA software v4.2.1 from the Broad Institute. Genes in *Tet2*-KO vs WT cells with or without IL1β were ranked by the sign of the log fold change in gene expression multiplied by the negative log base ten of the p value. Analysis was performed using Mouse_Gene_Symbol_Remapping_MSigDB.v7.0. Molecular signature databases include the Broad Institutes' "C2.all.v7.4symbols", as well as the literature derived genes identified as markers of the aged specific LT-HSCs cluster[22] with the ChIP platform Mouse_Gene_Symbol_Remapping_MSigDB.v7.0.

Enrichr and STRING analyses

For transcriptional data, statistically significant genes below a ($q < 0.05$) which were upregulated in *Tet2*-KO versus WT HSCs in either vehicle or IL1β treated mice were used for Enrichr analysis using "KEGG 2021 Human" dataset. For methylation data genes within 5000 base pairs of differentially methylated genes were utilized. STRING analysis (v11.5) was performed using genes significantly upregulated ($q < 0.05$) in *Tet2*-KO versus WT in both vehicle or IL1β treated mice. Data is from "Multiple proteins" analysis using mus musculus data and unconnected nodes by the full STRING network were removed. Gene ontology and KEGG pathway analysis was used from STRING analysis.

HOMER

Differentially methylated regions of interest spanning 50 CpG length tiles described above in this manuscript with a statistically significant increase or decrease of at least 10% in methylation level in *Tet2*-KO relative to WT were used as input for Homer's findMotifsGenome.pl script along with the mouse reference genome GRCm38. DMRs containing motifs of interest were determined by using Homer's annotatePeaks.pl script with the genes/DMRs and motif results.

Statistical analysis

Variables were compared by pairwise Student's two tailed t-test using the Microsoft excel software assuming homoscedastic variances: (*): $p<0.05$; (**): $p<0.01$; (***): $p<0.001$; (****): $p<0.0001$. For single cell RNA sequencing p values were adjusted Benjamini-Hochberg through DESeq2 to produce false discovery rate adjusted q values. Similarly, bisulfite sequencing by 50 CpG tiling for differentiation methylation by SeqMonk, as well as HOMER, STRING, and EnrichR were each

adjusted for false discovery rate (FDR) by their respective software. Orthogonal experimental model systems and approaches were taken to ensure the reproducibility of findings.

Acknowledgements

We thank OHSU Massively Parallel Sequencing Shared Resource, Flow Cytometry Core, and OHSU department of comparative medicine for their support. Funding for this project was provided by the American Cancer Society (RSG-17-187-01-LIB) as a research scholar award (AA) as well as Knight Cancer Research Institute and Cancer early detection advanced research center (Oregon Health & Science University) as pilot research projects. AA is also supported by grants from the National Cancer Institute (R01 CA229875-01A1), National Heart, Lung, and Blood Institute (R01 HL155426-01), Alex Lemonade /Babich RUNX1 Foundation, EvansMDS Foundation, and V foundation Scholar award (AA). JM is supported by Cancer Biology Student stipend grant.

Authorship Contributions

AA provided project oversight for experimental design, data analysis, interpretation, and methods development; JM, HL, MM, EW, CE, DG, and AA performed all the experiments and analyzed the data. RS, JM, AA, and HM performed single cell and whole genome bisulfite sequencing experiments and analysis. All of the authors wrote the manuscripts and provided feedback.

Disclosure of Conflicts of Interest: The authors declare no competing interests.

Supplementary Information: See separate documents.

Figure Legends

Figure 1: Chronic IL1β exposure enhances expansion of *Tet2*-KO cells and biases them towards neutrophil and ly6c^{hi} monocyte/macrophage production.

(a-c) *Tet2$^{fl/fl}$* (WT) and *Vav-Cre Tet$^{fl/fl}$* (*Tet2*-KO) mice were treated with IL1β (500 ng/mouse/day) or vehicle (n = 4 mice/group) for five weeks and peripheral blood (PB), bone marrow (BM) and spleen samples were analyzed by flow cytometry: **(a)** Experimental design, **(b)** spleen weight in grams (left) and the percentage of the PB CD45$^+$ cells which are myeloid (CD45$^+$CD11b$^+$, right), and **(c)** neutrophils (CD45$^+$CD11b$^+$Ly6c^{int}Ly6g$^+$), ly6c^{hi} monocytes/macrophages (CD45$^+$CD11b$^+$Ly6c$^+$Ly6g$^-$) and ly6c^{lo} monocytes/macrophages (CD45$^+$CD11b$^+$Ly6c$^-$Ly6g$^-$) in spleen cells at week five. (**d-f)** Lineage depleted BM cells from wild-type (WT) CD45.1$^+$ and *Rosa-rtTA*-driven inducible *Tet2* knockdown (*shTet2*) CD45.2 mice transplanted into lethally irradiated wild-type CD45.1$^+$CD45.2$^+$ mice subsequently treated with doxycycline (dox) and IL1β or vehicle for 4 weeks and then with and without doxycycline (withdrawal) for additional two weeks, analyzed by flow cytometry (n = 4-5 mice/group): **(d)** Experimental design, **(e)** percentage of WT CD45.1 and *shTet2* GFP$^+$CD45.2 cells out of CD45$^+$ (chimerism) and the percentage of WT CD45.1 and *shTet2* GFP$^+$CD45.2$^+$ cells which are myeloid (CD11b$^+$) in the PB for doxy and IL1β or vehicle treated experimental arms, **(f)** neutrophils, ly6c^{hi} monocytes/macrophages, and ly6c^{lo} monocytes/macrophages in the spleen with doxy or doxy withdrawal (w/d) for IL1β or vehicle treatments. Error bars represent mean ± SEM. Student's two tailed t-Test was used to determine significance: *$p < 0.05$, **$p < 0.01$, ***$p < 0.001$, ****$p < 0.0001$.

Figure 2: IL1β drives expansion and myeloid bias of *Tet2*-KO HSPCs.

WT and *Tet2*-KO mice (Fig. 1a) were treated with IL1β or vehicle (n = 4 mice/group) for five weeks and peripheral blood (PB), bone marrow (BM) and spleen cells were analyzed by flow cytometry. Additionally, BM harvested from WT CD45.1 and *shTet2* CD45.2 mice transplanted into lethally irradiated wild-type $CD45.1^{+}CD45.2^{+}$ recipient mice subsequently treated with doxycycline (dox) and IL1β or vehicle for 4 weeks, then with dox or dox withdrawal (w/d) for additional 2 weeks (Fig. 1d, n = 4/5 mice/group), analyzed by flow cytometry. **(a-c)** Percentage of live cells which are **(a)** LT-HSCs or ST-HSCs in the BM and spleen of *Tet2*-KO and WT mice, **(b)** LT-HSCs from WT CD45.1 or *shTet2* CD45.2 donor BM, **(c)** MPP2, MPP3, or MPP4 in the BM or spleen of WT and *Tet2*-KO mice. **(d)** Percentage of MPP2 (red), MPP3 (blue), or MPP4 (green) out of all MPP2-4 cells for WT CD45.1 or *shTet2* CD45.2 donor cells in BM and spleen. **(e)** Percentage of live $CD45^{+}$ cells which are MPP3 cells out of WT CD45.1 or *shTet2* CD45.2 BM donor cells. **(f)** The ratio of the frequency of GMPs and MEPs out of all live $CD45^{+}$ cells in *Tet2*-KO or WT mouse BM and spleens. **(g)** Simplified hematopoietic hierarchy with red text representing subsets elevated in frequency in *Tet2*-KO relative to WT mice treated with IL1β with red arrows connecting elevated subsets. Error bars represent mean ± SEM. Student's two tailed t-Test was used to determine significance: *$p < 0.05$, **$p < 0.01$, ***$p < 0.001$, ****$p < 0.0001$.

Figure 3: IL1β stimulation enhanced the self-renewal ability of *Tet2*-KO HSPCs while exhausting WT HSPCs. (a) *In vitro* competition of LSKs purified from BM harvested from CD45.1 WT and CD45.2 *Tet2*-KO mice. Cells were treated with or without IL1β and the percentage of Lin-, LK, and LSK cells was analyzed by flow cytometry analysis (n = 6 biological replicates). **(b)** Flow cytometry analysis of LSK and LK cells isolated from the BM of *Tet2*-KO and WT mice treated with and without IL1β for 4 weeks, with cell cycle proportions (left) and

representative gating of cell cycle using KI-67 and DAPI for LSK (right, n = 4 mice/group). **(c)** Colony-forming unit (CFU) assay of sorted LSK cells from WT or *Tet2*-KO BM (n = 9 technical replicates with 3 biological replicates). Colonies were counted and the cells re-plated every 7 days. M: macrophage; G: granulocyte; GM: granulocyte/macrophage; BFU-E: erythroid. Error bars represent mean ± SEM. Student's two tailed t-Test was used to determine significance: *$p < 0.05$, **$p < 0.01$, ***$p < 0.001$, ****$p < 0.0001$.

Figure 4: *Tet2*-KO HSCs exhibit transcriptional signatures for self-renewal capacity under inflammatory stress. (a) WT and *Tet2*-KO mice were treated for 5 weeks with and without IL1β (n = 4 mice/group). BM cells were harvested and lineage cells were depleted by magnetic selection. Cells were analyzed by 10X single cell RNA (scRNA) sequencing. **(b)** UMAP of 54,984 cells representing 17 clusters and bar graph representing their proportions including hematopoietic stem cell (HSC), progenitor (Prog), immature myeloid progenitor (IMP), granulocyte or monocyte progenitor (Gran/Mono Prog), monocyte (Mono), macrophage (Mac), neutrophil (Neut), basophil (Baso), megakaryocyte progenitor (MegP), common lymphoid progenitor (CLP), T cell (T-cell), plasmacytoid dendritic cells and B cell (pDc/B-cell), eosinophil (Eo), megakaryocyte-erythroid progenitor (MEP), colony-forming unit erythroid (CFU-E), erythroblast $CD45^-$ EryB (EryB_CD45-) and erythroblast $CD45^+$ EryB (EryB_CD45+). **(c)** Venn diagram of differentially expressed genes (DEGs) in *Tet2*-KO HSCs relative to WT treated with vehicle or IL1β. **(d)** Volcano plot with DEGs in *Tet2*-KO relative to WT HSCs with or without IL1β stimulations. Select genes based on enriched pathways are labelled. P adjusted values were determined using DESeq2. **(e)** Gene-set enrichment analysis (GSEA) from HSCs in *Tet2*-KO relative to WT showing significantly enriched genes (FDR < 0.05), with IL1β (red) or vehicle (black) or pathways

not significantly enriched in vehicle (grey). q values were determined by GSEA. **(f)** Enrichment of transcriptional signature specific to old HSCs within HSCs[22]. **(g)** UMAP visualization of the scRNA-seq data from combined (*Tet2*-KO and WT HSCs with or without IL1β) with cells colored by pseudotime inferred by Monocle3 trajectory inference on clusters. Student's two tailed t-Test was used to determine significance except where otherwise specified in the figure legend: *p < 0.05, **p < 0.01, ***p < 0.001, ****p < 0.0001.

Figure 5: Resistance to IL1β driven demethylation in *Tet2*-KO progenitors promotes differential hypermethylation associated with cellular fate. WT and *Tet2*-KO mice were treated for 5 weeks with and without IL1β (n = 4 mice/group). BM cells were harvested and LSK, CMP, and GMPs were purified and analyzed by whole genome bisulfite sequencing. **(a)** differentially methylated regions (DMRs) from 50 CpG long regions of the whole genome (>10% methylation difference, q < 0.05, determined by SeqMonk) between *Tet2*-KO and WT LSKs with or without IL1β stimulation. Bar plots below show the methylation level of all probes for each condition. **(b)** Percentage of 50 CpG segments overlapping each genomic element which are hypermethylated or hypomethylated DMRs in *Tet2*-KO relative to WT. **(c)** Percentage methylation difference between *Tet2*-KO and WT cells analyzed using literature derived ChIP-seq binding sites for each TF. **(d)** Top panel, MA plots showing methylation difference for LSK and CMP cells derived from *Tet2*-KO and WT mice treated with IL1β using literature derived ChIP-seq binding sites of terminal differentiation promoting transcription factors (TFs). The percentage of sites with higher methylation in *Tet2*-KO than WT are shown in the top right corner of each graph. Bottom panel, significance of motif enrichment using HOMER analysis tool within DMRs for TFs with and without IL1β stimulation. **(e)** Heatmap of the 150 most downregulated genes near

hypermethylated TFs binding motifs in *Tet2*-KO HSCs relative to WT treated with and without IL1β. Their differential expression is shown across HSC, Progenitors, and IMP clusters. Student's two tailed t-Test was used to determine significance except where otherwise specified in the figure legend: *p < 0.05, **p < 0.01, ***p < 0.001, ****p < 0.0001.

Figure 6: IL1R1 antagonism abrogates aberrant myeloid expansion in *Tet2*-KO mice. (a-c) Analysis of the PB of WT (n=8), *Vav-cre Tet2*$^{fl/fl}$ (*Tet2*-KO, n=10), *Il1r1*-/- (*Il1r1*-KO, n= 17), and *Vav-cre Tet2*$^{fl/fl}$*Il1r1*$^{-/-}$ (double knockout: DKO, n=13) mice between 20 – 60 weeks of age. **(a)** Experimental design. **(b)** Differential blood counts of white blood cells, and the percentage of neutrophils, monocytes, and lymphocytes. **(c)** Flow cytometry analysis showing percentage of Ly6c^{hi} monocytes out of CD45^{+} cells correlated with age of the mouse in weeks. **(d-g)** Lineage depleted BM cells derived from WT CD45.1 and *Tet2*-KO CD45.2 mice were transplanted into lethally irradiated WT CD45.1/2 mice. Mice were subsequently treated with IL1β (500 ng/mouse/day) or vehicle as well as with or without an IL1R1 antagonist (anakinra, 100mg/kg) (n = 3-4 mice/group): **(d)** experimental design, **(e)** percentage of *Tet2*-KO CD45.2 donor cells out of all CD45^{+} cells (chimerism) in PB. The percentage of WT CD45.1 donor cells out of all CD45^{+} cells are shown in Supplemental Figure 9C, **(f)** percentage of WT CD45.1 and *Tet2*-KO CD45.2 donor cells which are myeloid in the PB, **(g)** spleen weight, and percentage of LK cells out of all WT CD45.1 and *Tet2*-KO CD45.2 donor cells in spleen. **(h)** Human CD34^{+} progenitors were CRISPR-Cas9 edited for *TET2* (*TET2*-sgRNA) alongside non-targeting control (NT-sgRNA), then 600 cells per well were plated with or without IL1β (25ng/mL) and/or IL1RA (50ng/mL). Colonies were counted after 2 weeks and individual colonies were picked for sanger sequencing to

determine indel frequency within *TET2*. **(h)** Experimental design, and total colony numbers at 2 weeks and CFU-M (monocyte) colony numbers, with the number of colonies identified with detectable indels are shown. Error bars represent mean ± SEM. Student's two tailed t-Test was used to determine significance: *$p < 0.05$, **$p < 0.01$, ***$p < 0.001$, ****$p < 0.0001$.

REFERENCES

1. Genovese, G., *et al.* Clonal hematopoiesis and blood-cancer risk inferred from blood DNA sequence. *N Engl J Med* **371**, 2477-2487 (2014).
2. Buscarlet, M., *et al.* DNMT3A and TET2 dominate clonal hematopoiesis and demonstrate benign phenotypes and different genetic predispositions. *Blood* **130**, 753-762 (2017).
3. Jaiswal, S., *et al.* Clonal Hematopoiesis and Risk of Atherosclerotic Cardiovascular Disease. *N Engl J Med* **377**, 111-121 (2017).
4. Wang, Y., *et al.* Tet2-mediated clonal hematopoiesis in nonconditioned mice accelerates age-associated cardiac dysfunction. *JCI Insight* **5**, e135204 (2020).
5. Jaiswal, S., *et al.* Age-related clonal hematopoiesis associated with adverse outcomes. *N Engl J Med* **371**, 2488-2498 (2014).
6. Moran-Crusio, K., *et al.* Tet2 loss leads to increased hematopoietic stem cell self-renewal and myeloid transformation. *Cancer Cell* **20**, 11-24 (2011).
7. Cai, Z., *et al.* Inhibition of Inflammatory Signaling in Tet2 Mutant Preleukemic Cells Mitigates Stress-Induced Abnormalities and Clonal Hematopoiesis. *Cell Stem Cell* **23**, 833-849.e835 (2018).
8. Meisel, M., *et al.* Microbial signals drive pre-leukaemic myeloproliferation in a Tet2-deficient host. *Nature* **557**, 580-584 (2018).
9. Zeng, H., *et al.* Antibiotic treatment ameliorates Ten-eleven translocation 2 (TET2) loss-of-function associated hematological malignancies. *Cancer Lett* **467**, 1-8 (2019).
10. Abegunde, S.O., Buckstein, R., Wells, R.A. & Rauh, M.J. An inflammatory environment containing TNFα favors Tet2-mutant clonal hematopoiesis. *Experimental Hematology* **59**, 60-65 (2018).
11. Ridker, P.M., *et al.* Effect of interleukin-1β inhibition with canakinumab on incident lung cancer in patients with atherosclerosis: exploratory results from a randomised, double-blind, placebo-controlled trial. *The Lancet* **390**, 1833-1842 (2017).
12. Hosseini, M.M., *et al.* Inhibition of interleukin-1 receptor-associated kinase-1 is a therapeutic strategy for acute myeloid leukemia subtypes. *Leukemia* (2018).
13. Carey, A., *et al.* Identification of Interleukin-1 by Functional Screening as a Key Mediator of Cellular Expansion and Disease Progression in Acute Myeloid Leukemia. *Cell Rep* **18**, 3204-3218 (2017).
14. Sano, S., *et al.* Tet2-Mediated Clonal Hematopoiesis Accelerates Heart Failure Through a Mechanism Involving the IL-1β/NLRP3 Inflammasome. *J Am Coll Cardiol* **71**, 875-886 (2018).
15. Bick, A.G., *et al.* Inherited causes of clonal haematopoiesis in 97,691 whole genomes. *Nature* **586**, 763-768 (2020).
16. Jaiswal, S. Clonal hematopoiesis and risk of atherosclerotic cardiovascular disease. *N. Engl. J. Med.* **377**(2017).
17. Jafri, S., Moore, S.D., Morrell, N.W. & Ormiston, M.L. A sex-specific reconstitution bias in the competitive CD45.1/CD45.2 congenic bone marrow transplant model. *Sci Rep* **7**, 3495 (2017).

18. Cimmino, L., *et al.* Restoration of TET2 Function Blocks Aberrant Self-Renewal and Leukemia Progression. *Cell* **170**, 1079-1095.e1020 (2017).
19. Ye, M., *et al.* Hematopoietic Stem Cells Expressing the Myeloid Lysozyme Gene Retain Long-Term, Multilineage Repopulation Potential. *Immunity* **19**, 689-699 (2003).
20. Pietras, E.M., *et al.* Chronic interleukin-1 exposure drives haematopoietic stem cells towards precocious myeloid differentiation at the expense of self-renewal. *Nat Cell Biol* **18**, 607-618 (2016).
21. Trumpp, A., Essers, M. & Wilson, A. Awakening dormant haematopoietic stem cells. *Nature Reviews Immunology* **10**, 201-209 (2010).
22. Kirschner, K., *et al.* Proliferation Drives Aging-Related Functional Decline in a Subpopulation of the Hematopoietic Stem Cell Compartment. *Cell Rep* **19**, 1503-1511 (2017).
23. Jung, H., *et al.* TXNIP Maintains the Hematopoietic Cell Pool by Switching the Function of p53 under Oxidative Stress. *Cell Metabolism* **18**, 75-85 (2013).
24. Mallaney, C., *et al.* Kdm6b regulates context-dependent hematopoietic stem cell self-renewal and leukemogenesis. *Leukemia* **33**, 2506-2521 (2019).
25. Knudsen, K.J., *et al.* ERG promotes the maintenance of hematopoietic stem cells by restricting their differentiation. *Genes Dev* **29**, 1915-1929 (2015).
26. Ariki, R., *et al.* Homeodomain transcription factor Meis1 is a critical regulator of adult bone marrow hematopoiesis. *PloS one* **9**, e87646-e87646 (2014).
27. Min, I.M., *et al.* The Transcription Factor EGR1 Controls Both the Proliferation and Localization of Hematopoietic Stem Cells. *Cell Stem Cell* **2**, 380-391 (2008).
28. Takizawa, H., *et al.* Pathogen-Induced TLR4-TRIF Innate Immune Signaling in Hematopoietic Stem Cells Promotes Proliferation but Reduces Competitive Fitness. *Cell Stem Cell* **21**, 225-240.e225 (2017).
29. Wahlestedt, M., *et al.* Critical Modulation of Hematopoietic Lineage Fate by Hepatic Leukemia Factor. *Cell Rep* **21**, 2251-2263 (2017).
30. Kumar, P., *et al.* HMGA2 promotes long-term engraftment and myeloerythroid differentiation of human hematopoietic stem and progenitor cells. *Blood Adv* **3**, 681-691 (2019).
31. Izzo, F., *et al.* DNA methylation disruption reshapes the hematopoietic differentiation landscape. *Nature Genetics* **52**, 378-387 (2020).
32. Yamazaki, J., *et al.* TET2 Mutations Affect Non-CpG Island DNA Methylation at Enhancers and Transcription Factor-Binding Sites in Chronic Myelomonocytic Leukemia. *Cancer Res* **75**, 2833-2843 (2015).
33. Tulstrup, M., *et al.* TET2 mutations are associated with hypermethylation at key regulatory enhancers in normal and malignant hematopoiesis. *Nature Communications* **12**, 6061 (2021).
34. Ferreira, R., *et al.* Impaired in vitro erythropoiesis following deletion of the Scl (Tal1) +40 enhancer is largely compensated for in vivo despite a significant reduction in expression. *Molecular and cellular biology* **33**, 1254-1266 (2013).
35. Deen, D., *et al.* Identification of the transcription factor MAZ as a regulator of erythropoiesis. *Blood Adv* **5**, 3002-3015 (2021).
36. Chen, D. & Zhang, G. Enforced expression of the GATA-3 transcription factor affects cell fate decisions in hematopoiesis. *Experimental Hematology* **29**, 971-980 (2001).

37. Lacorazza, H.D., *et al.* The transcription factor MEF/ELF4 regulates the quiescence of primitive hematopoietic cells. *Cancer Cell* **9**, 175-187 (2006).
38. Dakic, A., Wu, L. & Nutt, S.L. Is PU.1 a dosage-sensitive regulator of haemopoietic lineage commitment and leukaemogenesis? *Trends in Immunology* **28**, 108-114 (2007).
39. Sato, A., *et al.* C/EBPβ Isoforms Regulate Proliferation and Differentiation of Regenerating Hematopoietic Stem/Progenitor Cells. *Blood* **134**, 3713-3713 (2019).
40. Xiao, X., *et al.* Targeting JNK pathway promotes human hematopoietic stem cell expansion. *Cell Discovery* **5**, 2 (2019).
41. Glaccum, M.B., *et al.* Phenotypic and functional characterization of mice that lack the type I receptor for IL-1. *The Journal of Immunology* **159**, 3364 (1997).
42. Ito, K., *et al.* Non-catalytic Roles of Tet2 Are Essential to Regulate Hematopoietic Stem and Progenitor Cell Homeostasis. *Cell Rep* **28**, 2480-2490.e2484 (2019).
43. Urien, S., *et al.* Anakinra pharmacokinetics in children and adolescents with systemic-onset juvenile idiopathic arthritis and autoinflammatory syndromes. *BMC Pharmacol Toxicol* **14**, 40-40 (2013).
44. Lang, R. & Raffi, F.A.M. Dual-Specificity Phosphatases in Immunity and Infection: An Update. *Int J Mol Sci* **20**, 2710 (2019).
45. Hayden, M.S. & Ghosh, S. Shared Principles in NF-κB Signaling. *Cell* **132**, 344-362 (2008).
46. Cull, A.H., Snetsinger, B., Buckstein, R., Wells, R.A. & Rauh, M.J. Tet2 restrains inflammatory gene expression in macrophages. *Experimental Hematology* **55**, 56-70.e13 (2017).
47. Tabas, I. & Lichtman, A.H. Monocyte-Macrophages and T Cells in Atherosclerosis. *Immunity* **47**, 621-634 (2017).
48. Ågerstam, H., *et al.* IL1RAP antibodies block IL-1–induced expansion of candidate CML stem cells and mediate cell killing in xenograft models. *Blood* **128**, 2683-2693 (2016).
49. Buckley, L.F. & Abbate, A. Interleukin-1 blockade in cardiovascular diseases: a clinical update. *European Heart Journal* **39**, 2063-2069 (2018).
50. Stuart, T., *et al.* Comprehensive Integration of Single-Cell Data. *Cell* **177**, 1888-1902.e1821 (2019).
51. Choi, J., *et al.* Haemopedia RNA-seq: a database of gene expression during haematopoiesis in mice and humans. *Nucleic Acids Res* **47**, D780-D785 (2019).
52. Giladi, A., *et al.* Single-cell characterization of haematopoietic progenitors and their trajectories in homeostasis and perturbed haematopoiesis. *Nat Cell Biol* **20**, 836-846 (2018).
53. Baccin, C., *et al.* Combined single-cell and spatial transcriptomics reveal the molecular, cellular and spatial bone marrow niche organization. *Nat Cell Biol* **22**, 38-48 (2020).
54. Clark, S.J., *et al.* Genome-wide base-resolution mapping of DNA methylation in single cells using single-cell bisulfite sequencing (scBS-seq). *Nature Protocols* **12**, 534-547 (2017).
55. Macaulay, I.C., *et al.* Separation and parallel sequencing of the genomes and transcriptomes of single cells using G&T-seq. *Nature Protocols* **11**, 2081-2103 (2016).
56. Picelli, S., *et al.* Smart-seq2 for sensitive full-length transcriptome profiling in single cells. *Nature Methods* **10**, 1096-1098 (2013).
57. Krueger, F. Quality Control, trimming and alignment of Bisulfite-Seq data (Prot 57). *Epigenesys* (2012).

58. Krueger, F. & Andrews, S.R. Bismark: a flexible aligner and methylation caller for Bisulfite-Seq applications. *Bioinformatics* **27**, 1571-1572 (2011).
59. Lara-Astiaso, D.*, et al.* Chromatin state dynamics during blood formation. *Science* **345**, 943-949 (2014).
60. Feng, J., Liu, T., Qin, B., Zhang, Y. & Liu, X.S. Identifying ChIP-seq enrichment using MACS. *Nature Protocols* **7**, 1728-1740 (2012).

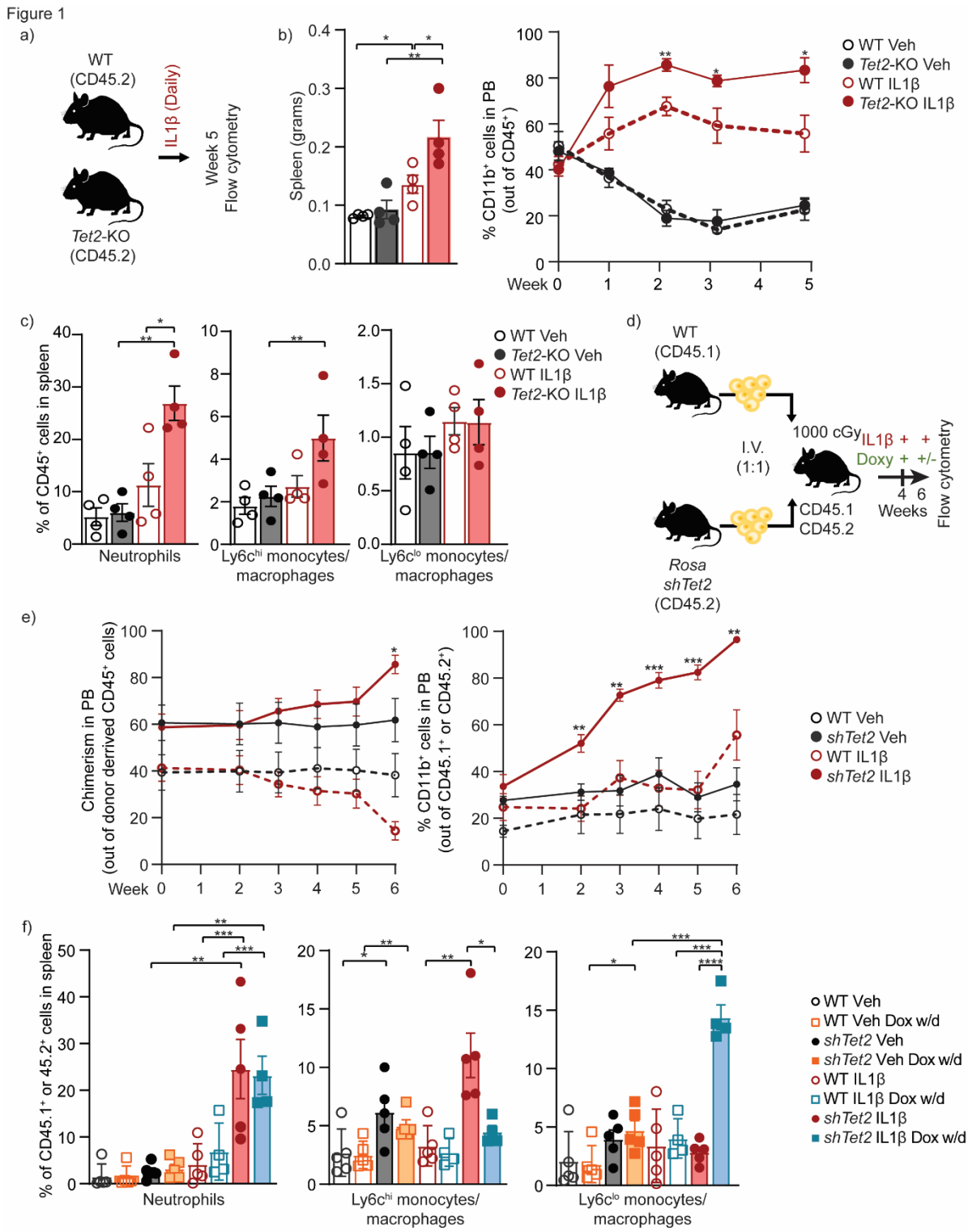

Figure 1: Chronic IL1β exposure enhances expansion of *Tet2*-KO cells and biases them towards neutrophil and ly6c^{hi} monocyte/macrophage production. (a-c) *Tet2$^{fl/fl}$* (WT) and *Vav-Cre Tet$^{fl/fl}$* (*Tet2*-KO) mice were treated with IL1β (500 ng/mouse/day) or vehicle (n = 4 mice/group) for five weeks and peripheral blood (PB), bone marrow (BM) and spleen samples were analyzed by flow cytometry: **(a)** Experimental design, **(b)** spleen weight in grams (left) and the percentage of the PB CD45$^+$ cells which are myeloid (CD45$^+$CD11b$^+$, right), and **(c)** neutrophils (CD45$^+$CD11b$^+$Ly6c^{int}Ly6g$^+$), ly6c^{hi} monocytes/macrophages (CD45$^+$CD11b$^+$Ly6c$^+$Ly6g$^-$) and ly6c^{lo} monocytes/macrophages (CD45$^+$CD11b$^+$Ly6c$^-$Ly6g$^-$) in spleen cells at week five. (**d-f)** Lineage depleted BM cells from wild-type (WT) CD45.1$^+$ and *Rosa-rtTA*-driven inducible *Tet2* knockdown (*shTet2*) CD45.2 mice transplanted into lethally irradiated wild-type CD45.1$^+$CD45.2$^+$ mice subsequently treated with doxycycline (dox) and IL1β or vehicle for 4 weeks and then with and without doxycycline (withdrawal) for additional two weeks, analyzed by flow cytometry (n = 4-5 mice/group): **(d)** Experimental design, **(e)** percentage of WT CD45.1 and *shTet2* GFP$^+$CD45.2 cells out of CD45$^+$ (chimerism) and the percentage of WT CD45.1 and *shTet2*

$GFP^{+}CD45.2^{+}$ cells which are myeloid ($CD11b^{+}$) in the PB for doxy and IL1β or vehicle treated experimental arms, **(f)** neutrophils, $ly6c^{hi}$ monocytes/macrophages, and $ly6c^{lo}$ monocytes/macrophages in the spleen with doxy or doxy withdrawal (w/d) for IL1β or vehicle treatments. Error bars represent mean ± SEM. Student's two tailed t-Test was used to determine significance: *$p < 0.05$, **$p < 0.01$, ***$p < 0.001$, ****$p < 0.0001$.

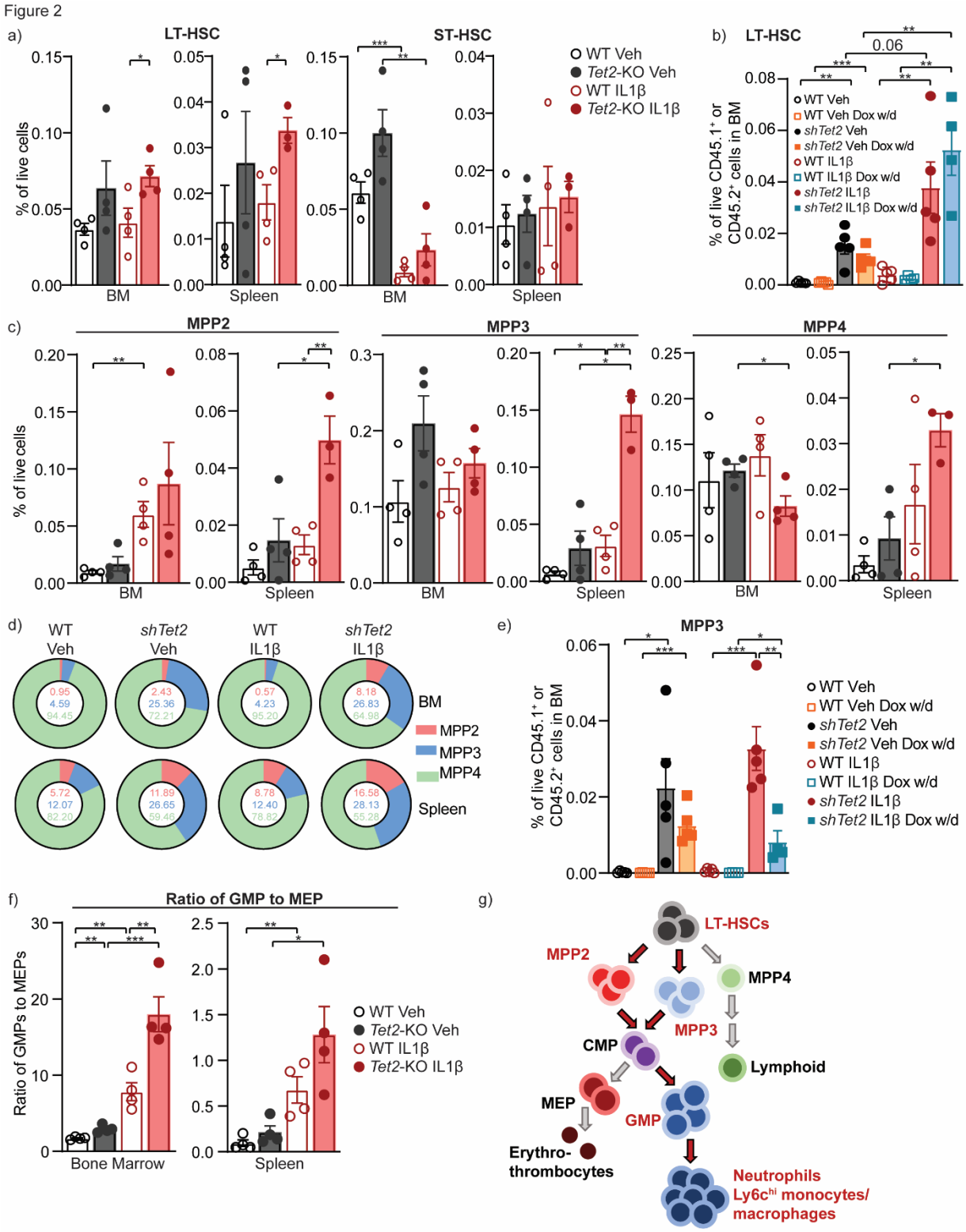

Figure 2: IL1β drives expansion and myeloid bias of *Tet2*-KO HSPCs. WT and *Tet2*-KO mice (Fig. 1a) were treated with IL1β or vehicle (n = 4 mice/group) for five weeks and peripheral blood (PB), bone marrow (BM) and spleen cells were analyzed by flow cytometry. Additionally, BM harvested from WT CD45.1 and *shTet2* CD45.2 mice transplanted into lethally irradiated wild-type CD45.1$^+$CD45.2$^+$ recipient mice subsequently treated with doxycycline (dox) and IL1β or vehicle for 4 weeks, then with dox or dox withdrawal (w/d) for additional 2 weeks (Fig. 1d, n = 4/5 mice/group), analyzed by flow cytometry. **(a-c)** Percentage of live cells which are **(a)** LT-HSCs or ST-HSCs in the BM and spleen of *Tet2*-KO and WT mice, **(b)** LT-HSCs from WT CD45.1 or *shTet2* CD45.2 donor BM, **(c)** MPP2, MPP3, or MPP4 in the BM or spleen of WT and *Tet2*-KO mice. **(d)** Percentage of MPP2 (red), MPP3 (blue), or MPP4 (green) out of all MPP2-4 cells for WT CD45.1 or *shTet2* CD45.2 donor cells in BM and spleen. **(e)** Percentage of live CD45$^+$ cells which are MPP3 cells out of WT CD45.1 or *shTet2* CD45.2 BM donor cells. **(f)** The ratio of the frequency of GMPs and MEPs out of all live CD45$^+$

cells in *Tet2*-KO or WT mouse BM and spleens. **(g)** Simplified hematopoietic hierarchy with red text representing subsets elevated in frequency in *Tet2*-KO relative to WT mice treated with IL1β with red arrows connecting elevated subsets. Error bars represent mean ± SEM. Student's two tailed t-Test was used to determine significance: *$p < 0.05$, **$p < 0.01$, ***$p < 0.001$, ****$p < 0.0001$.

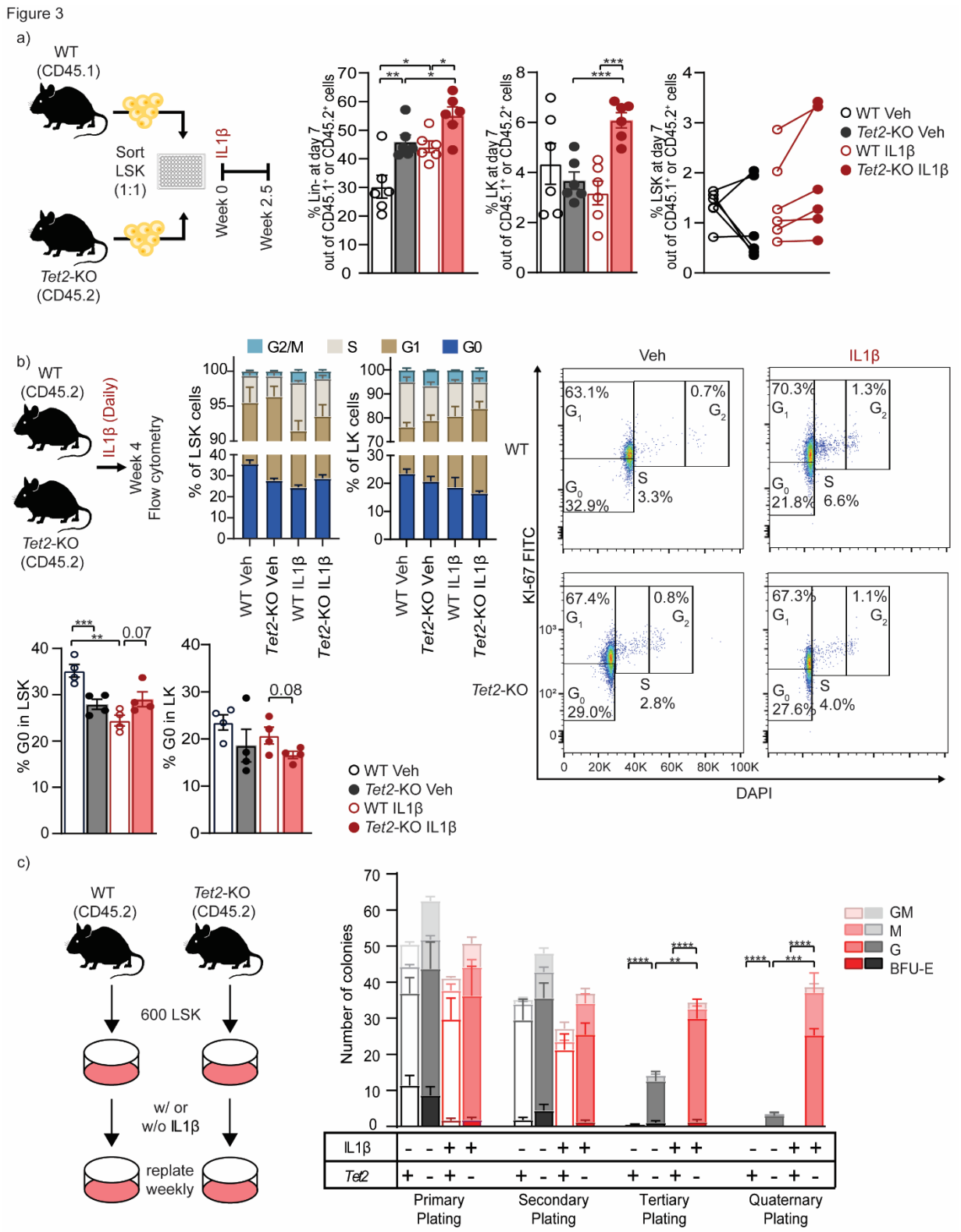

Figure 3: IL1β stimulation enhanced the self-renewal ability of *Tet2*-KO HSPCs while exhausting WT HSPCs. (a) *In vitro* competition of LSKs purified from BM harvested from CD45.1 WT and CD45.2 *Tet2*-KO mice. Cells were treated with or without IL1β and the percentage of Lin-, LK, and LSK cells was analyzed by flow cytometry analysis (n = 6 biological replicates). **(b)** Flow cytometry analysis of LSK and LK cells isolated from the BM of *Tet2*-KO and WT mice treated with and without IL1β for 4 weeks, with cell cycle proportions (left) and representative gating of cell cycle using KI-67 and DAPI for LSK (right, n = 4 mice/group). **(c)** Colony-forming unit (CFU) assay of sorted LSK cells from WT or *Tet2*-KO BM (n = 9 technical replicates with 3 biological replicates). Colonies were counted and the cells re-plated every 7 days. M: macrophage; G: granulocyte; GM: granulocyte/macrophage; BFU-E: erythroid. Error bars represent mean ± SEM. Student's two tailed t-Test was used to determine significance: *p < 0.05, **p < 0.01, ***p < 0.001, ****p < 0.0001.

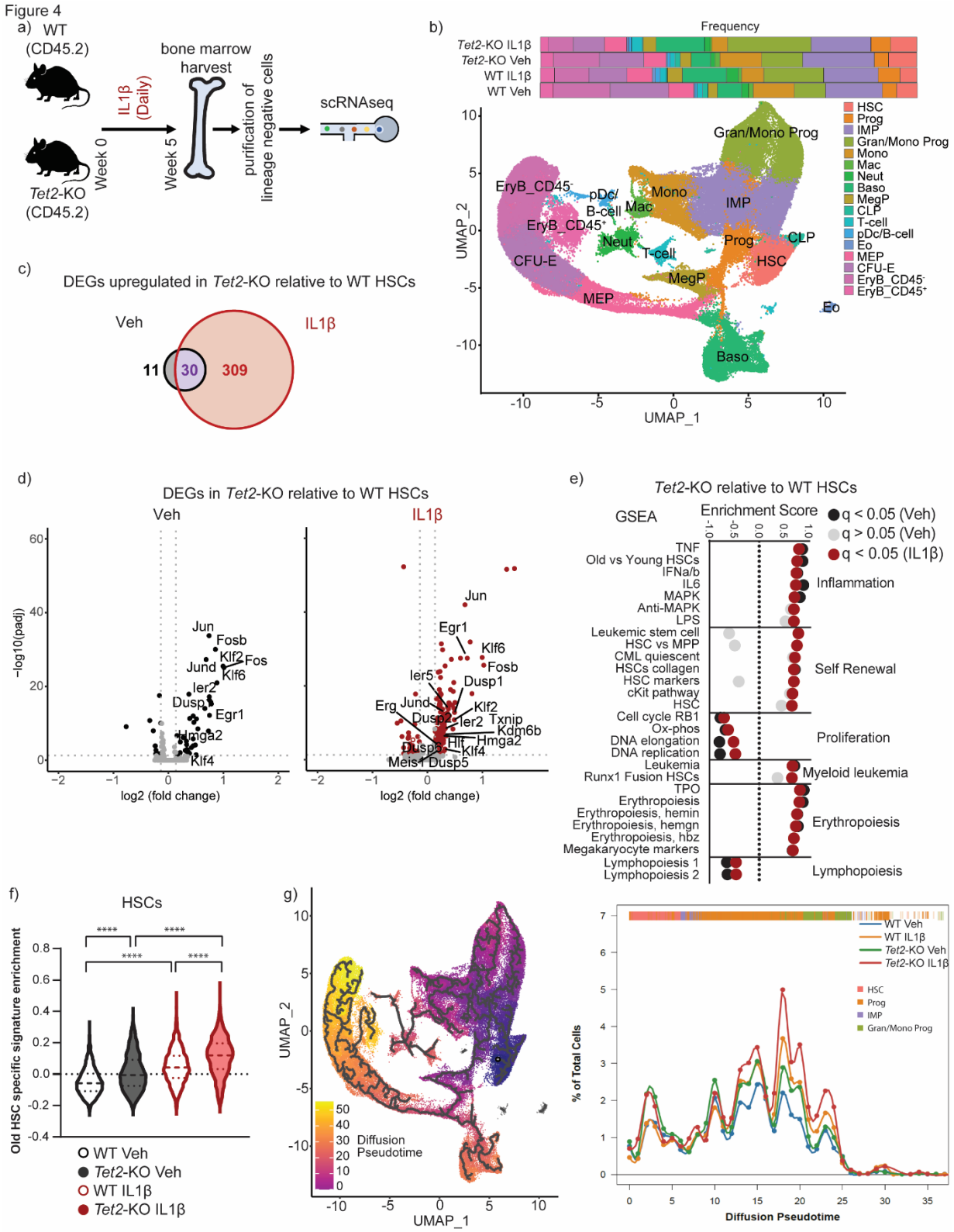

Figure 4: *Tet2*-KO HSCs exhibit transcriptional signatures for self-renewal capacity under inflammatory stress. (a) WT and *Tet2*-KO mice were treated for 5 weeks with and without IL1β (n = 4 mice/group). BM cells were harvested and lineage cells were depleted by magnetic selection. Cells were analyzed by 10X single cell RNA (scRNA) sequencing. **(b)** UMAP of 54,984 cells representing 17 clusters and bar graph representing their proportions including hematopoietic stem cell (HSC), progenitor (Prog), immature myeloid progenitor (IMP), granulocyte or monocyte progenitor (Gran/Mono Prog), monocyte (Mono), macrophage (Mac), neutrophil (Neut), basophil (Baso), megakaryocyte progenitor (MegP), common lymphoid progenitor (CLP), T cell (T-cell), plasmacytoid dendritic cells and B cell (pDc/B-cell), eosinophil (Eo), megakaryocyte-erythroid progenitor (MEP), colony-forming unit erythroid (CFU-E), erythroblast CD45$^-$ EryB

(EryB_CD45-) and erythroblast CD45^{+} EryB (EryB_CD45+). **(c)** Venn diagram of differentially expressed genes (DEGs) in *Tet2*-KO HSCs relative to WT treated with vehicle or IL1β. **(d)** Volcano plot with DEGs in *Tet2*-KO relative to WT HSCs with or without IL1β stimulations. Select genes based on enriched pathways are labelled. P adjusted values were determined using DESeq2. **(e)** Gene-set enrichment analysis (GSEA) from HSCs in *Tet2*-KO relative to WT showing significantly enriched genes (FDR < 0.05), with IL1β (red) or vehicle (black) or pathways not significantly enriched in vehicle (grey). q values were determined by GSEA. **(f)** Enrichment of transcriptional signature specific to old HSCs within HSCs[21]. **(g)** UMAP visualization of the scRNA-seq data from combined (*Tet2*-KO and WT HSCs with or without IL1β) with cells colored by pseudotime inferred by Monocle3 trajectory inference on clusters. Student's two tailed t-Test was used to determine significance except where otherwise specified in the figure legend: *p < 0.05, **p < 0.01, ***p < 0.001, ****p < 0.0001.

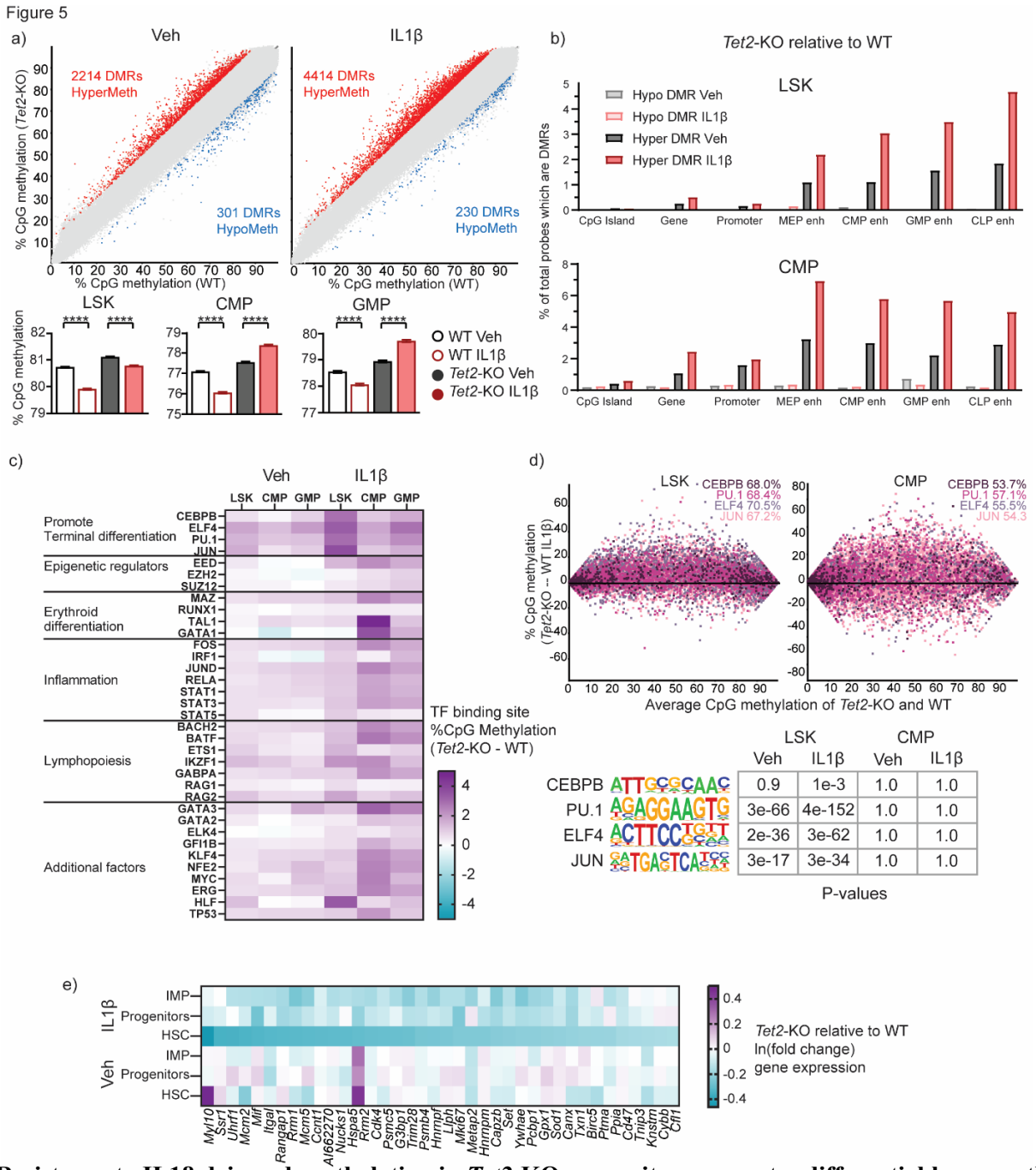

Figure 5: Resistance to IL1β driven demethylation in *Tet2*-KO progenitors promotes differential hypermethylation associated with cellular fate. WT and *Tet2*-KO mice were treated for 5 weeks with and without IL1β (n = 4 mice/group). BM cells were harvested and LSK, CMP, and GMPs were purified and analyzed by whole genome bisulfite sequencing. **(a)** differentially methylated regions (DMRs) from 50 CpG long regions of the whole genome (>10% methylation difference, $q < 0.05$, determined by SeqMonk) between *Tet2*-KO and WT LSKs with or without IL1β stimulation. Bar plots below show the methylation level of all probes for each condition. **(b)** Percentage of 50 CpG segments overlapping each genomic element which are hypermethylated or hypomethylated DMRs in *Tet2*-KO relative to WT. **(c)** Percentage methylation difference between *Tet2*-KO and WT cells analyzed using literature derived ChIP-seq binding sites for each TF. **(d)** Top panel, MA plots showing methylation difference for LSK and CMP cells derived from *Tet2*-KO and WT mice treated with IL1β using literature derived ChIP-seq binding sites of terminal differentiation promoting transcription factors (TFs). The percentage of sites with higher methylation in *Tet2*-KO than WT are shown in the top right corner of each graph. Bottom panel, significance of motif enrichment using HOMER analysis tool within DMRs for TFs with and without IL1β stimulation. **(e)** Heatmap of the 150 most downregulated genes near hypermethylated TFs binding motifs in *Tet2*-KO HSCs relative to WT treated with and without IL1β. Their differential expression is shown across HSC, Progenitors, and IMP clusters. Student's two tailed t-Test was used to determine significance except where otherwise specified in the figure legend: *$p < 0.05$, **$p < 0.01$, ***$p < 0.001$, ****$p < 0.0001$.

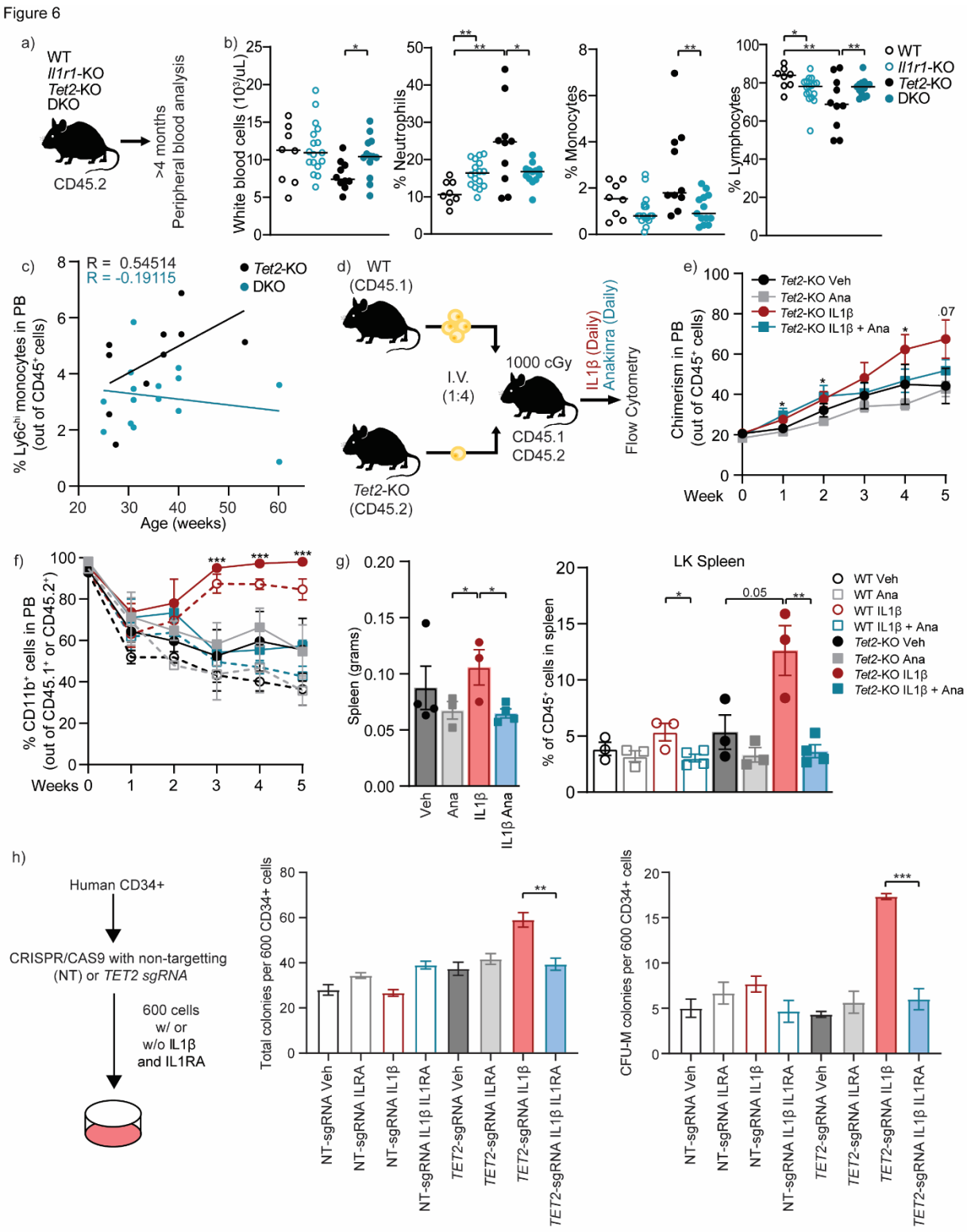

Figure 6: IL1R1 antagonism abrogates aberrant myeloid expansion in *Tet2*-KO mice. (a-c) Analysis of the PB of WT (n=8), *Vav-cre Tet2*$^{fl/fl}$ (*Tet2*-KO, n=10), *Il1r1*-/- (*Il1r1*-KO, n= 17), and *Vav-cre Tet2*$^{fl/fl}$*Il1r1*$^{-/-}$ (double knockout: DKO, n=13) mice between 20 – 60 weeks of age. **(a)** Experimental design. **(b)** Differential blood counts of white blood cells, and the percentage of neutrophils, monocytes, and lymphocytes. **(c)** Flow cytometry analysis showing percentage of Ly6c^{hi} monocytes out of CD45^{+} cells correlated with age of the mouse in weeks. **(d-g)** Lineage depleted BM cells derived from WT CD45.1 and *Tet2*-KO CD45.2 mice were transplanted into lethally irradiated WT CD45.1/2 mice. Mice were subsequently treated with IL1β (500 ng/mouse/day) or vehicle as well as with or without an IL1R1 antagonist (anakinra, 100mg/kg) (n = 3-4 mice/group): **(d)** experimental design, **(e)** percentage of *Tet2*-KO CD45.2 donor cells out of all CD45^{+} cells (chimerism) in PB. The percentage of WT CD45.1 donor cells out of all CD45^{+} cells are shown in Supplemental Figure

9C, **(f)** percentage of WT CD45.1 and *Tet2*-KO CD45.2 donor cells which are myeloid in the PB, **(g)** spleen weight, and percentage of LK cells out of all WT CD45.1 and *Tet2*-KO CD45.2 donor cells in spleen. **(h)** Human $CD34^+$ progenitors were CRISPR-Cas9 edited for *TET2* (*TET2*-sgRNA) alongside non-targeting control (NT-sgRNA), then 600 cells per well were plated with or without IL1β (25ng/mL) and/or IL1RA (50ng/mL). Colonies were counted after 2 weeks and individual colonies were picked for sanger sequencing to determine indel frequency within *TET2*. **(h)** Experimental design, and total colony numbers at 2 weeks and CFU-M (monocyte) colony numbers, with the number of colonies identified with detectable indels are shown. Error bars represent mean ± SEM. Student's two tailed t-Test was used to determine significance: *$p < 0.05$, **$p < 0.01$, ***$p < 0.001$, ****$p < 0.0001$.

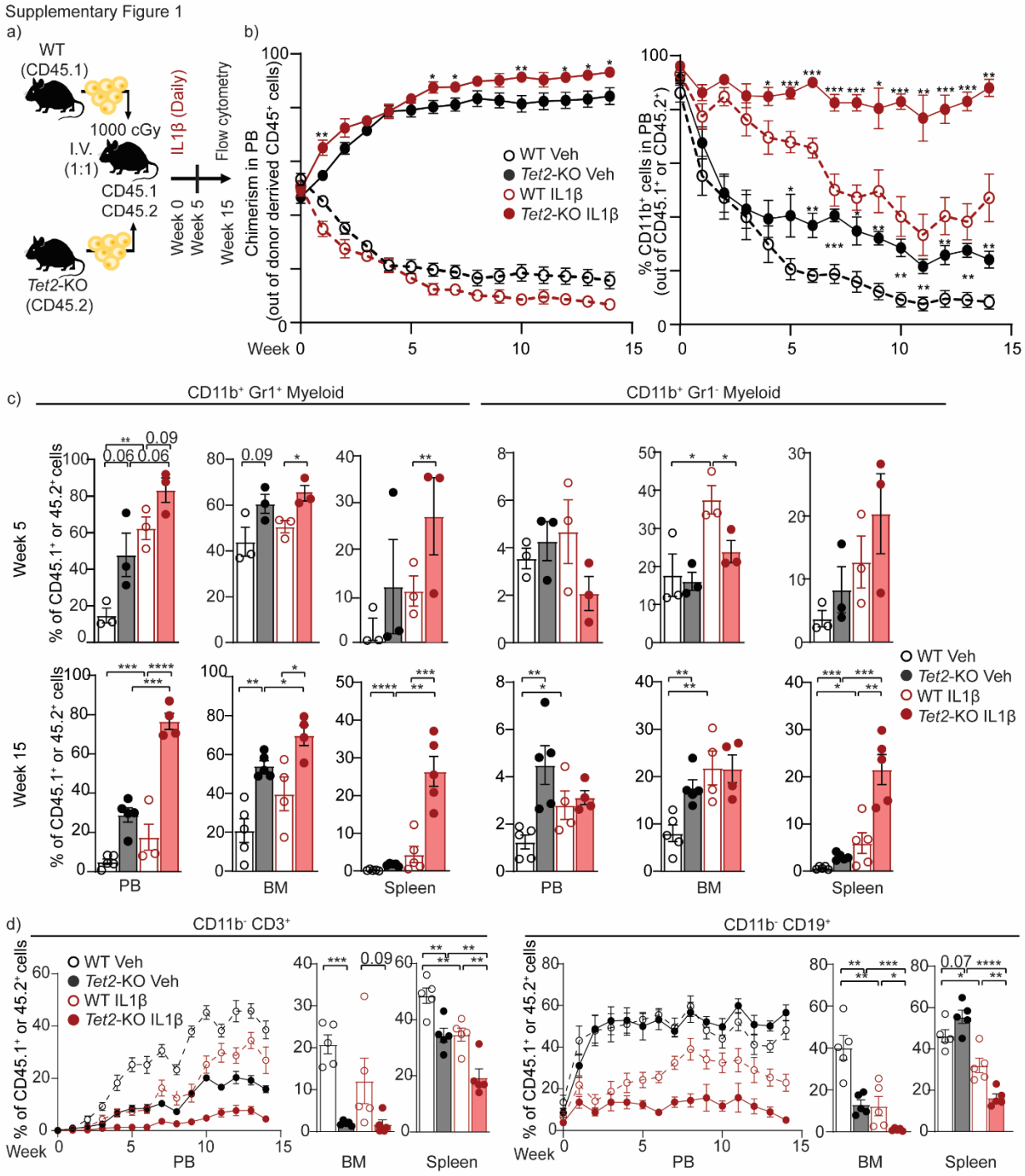

Supplementary Figure 1: Chronic IL1β exposure enhances myeloid expansion of *Tet2*-KO Gr1^{hi} positive cells at the expense of lymphopoiesis. (a-d) Lineage depleted BM cells from WT CD45.1 and *Tet2*-KO CD45.2 mice were transplanted into lethally irradiated WT CD45.1/2 mice subsequently treated with IL1β (500 ng/mouse/day) or vehicle daily. **(a)** Experimental design, **(b)** percentage of WT CD45.1 or *Tet2*-KO CD45.2 cells out of all CD45^{+} cells (chimerism, significance shown between Tet2-KO with and without IL1β treatment) and the percentage WT CD45.1 and *Tet2*-KO CD45.2^{+} cells which are myeloid in the PB (significance shown between Tet2-KO and WT with IL1β treatment), **(c)** myeloid subsets (CD11b^{+}Gr1^{hi}, CD11b^{+}Gr1^{lo}), and **(d)** T cells (CD11b^{-}CD3^{+}) and B cells (CD11b^{-}CD19^{+}) in PB, BM, and spleen (n = 3 mice/group for week 5; n = 4-5 mice/group for week 15). Error bars represent mean ± SEM. Student's two tailed t-Test was used to determine significance: *p < 0.05, **p < 0.01, ***p < 0.001, ****p < 0.0001.

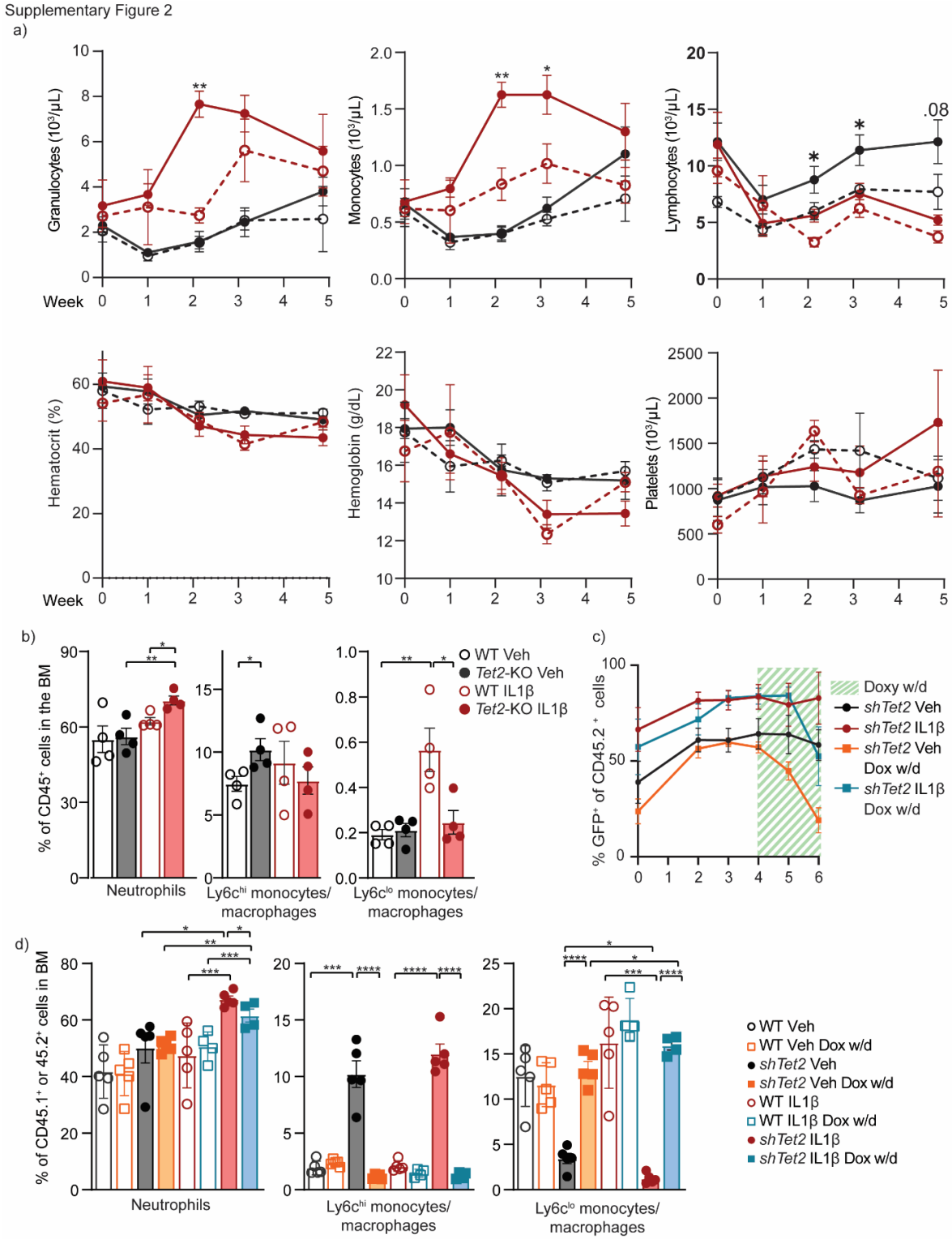

Supplementary Figure 2: Chronic IL1β exposure enhances myeloid expansion of *Tet2*-KO cells in multiple murine models. (a-b) *Tet2*$^{fl/fl}$ (WT) and *Vav-Cre Tet2*$^{fl/fl}$ (*Tet2*-KO) mice were treated with IL1β or vehicle (n = 4 mice/group) for five weeks (described in Fig. 1a): **(a)** Differential blood cell counts representing granulocytes, monocytes, lymphocytes, hematocrit, hemoglobin, and platelets in the PB, and **(b)** flow cytometric analysis representing the percentage of neutrophils, ly6c^{hi} monocytes/macrophages, and ly6c^{lo} monocytes/macrophages in the BM. **(c-d)** Lineage depleted BM cells from wild-type (WT) CD45.1^{+} and *Rosa-rtTA*-driven inducible *Tet2* knockdown (*shTet2*) mice transplanted into lethally irradiated wild-type CD45.1^{+}CD45.2^{+} mice subsequently treated with doxycycline (dox) and IL1β or vehicle, and then with and without doxycycline (withdrawal, w/d) for additional two weeks, analyzed by flow cytometry (n = 4-5 mice/group) (described in Fig. 1d) : **(c)** percentage of CD45^{+} *shTet2* which are GFP^{+} in PB **(d)** and the percentage of neutrophils, ly6c^{hi} monocytes/macrophages, and ly6c^{lo} monocytes/macrophages in the BM (n = 4-5 mice/group). Error bars represent mean ± SEM. Student's two tailed t-Test was used to determine significance: *p < 0.05, **p < 0.01, ***p < 0.001, ****p < 0.0001.

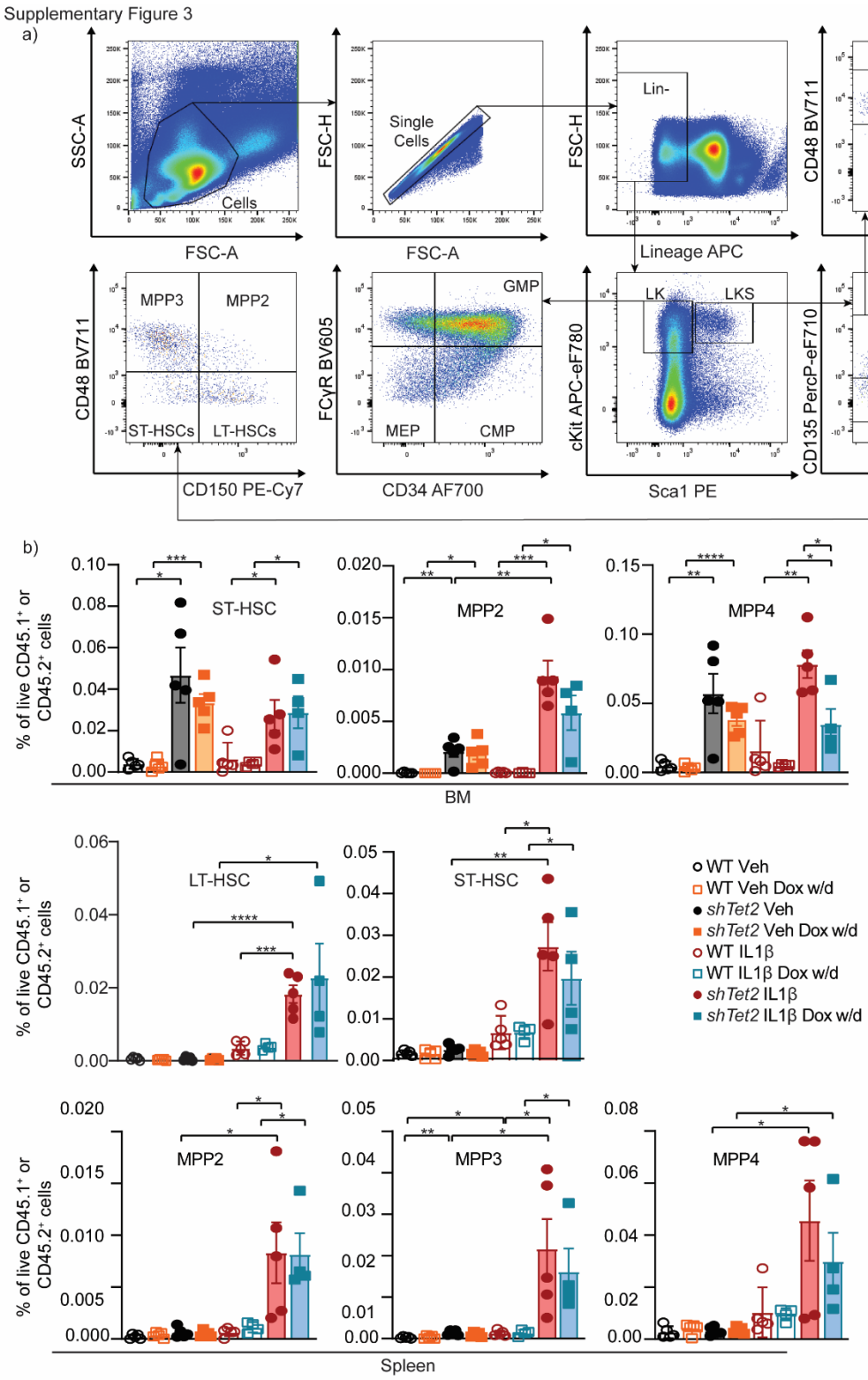

Supplementary Figure 3: IL1β stimulation promotes HSPC expansion in *Tet2* knockdown mice relative to WT in a competition repopulation experiment. (a) Representative gating scheme for HSPCs for flow cytometric analysis of the BM from a WT mouse. **(b)** Lineage depleted BM cells derived from WT CD45.1 and *shTet2* CD45.2 mice transplanted into lethally irradiated wild-type CD45.1^{+}CD45.2^{+} mice, mice were treated with doxycycline (dox) and IL1β or vehicle for 4 weeks, and then with doxy or doxy withdrawal (w/d) for two weeks (Fig. 1d) and analyzed by flow cytometry analysis. Percentage out of live (Cell trace violet-) cells gated out of WT CD45.1 and *shTet2* CD45.2 for ST-HSCs, MPP2s, MPP4s within BM and LT-HSCs, ST-HSCs, MPP2s, MPP3s, and MPP4s in BM or spleen of recipient mice (n = 4-5 mice/group). Error bars represent mean ± SEM. Student's two tailed t-Test was used to determine significance: *$p < 0.05$, **$p < 0.01$, ***$p < 0.001$, ****$p < 0.0001$.

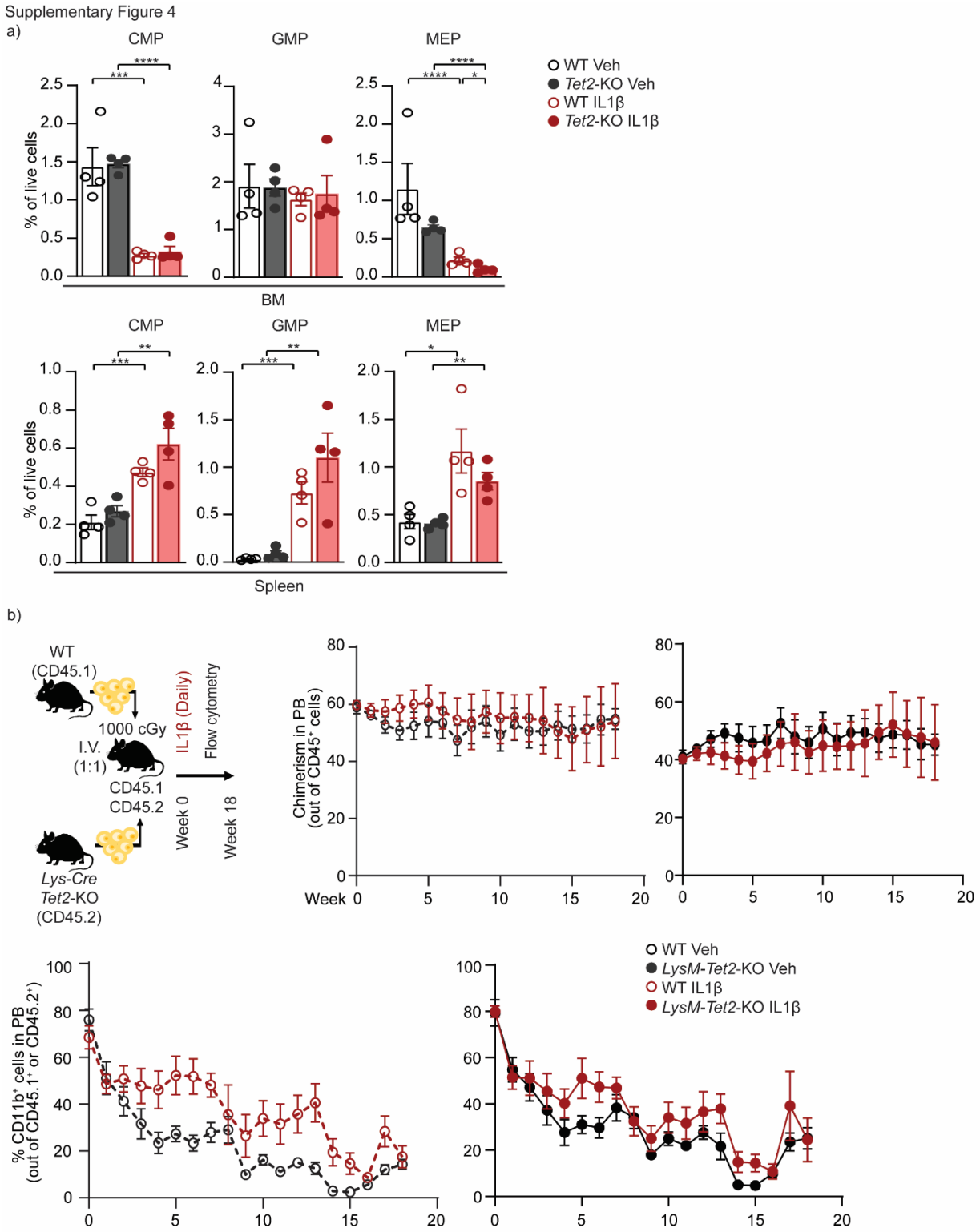

Supplementary Figure 4: IL1β stimulation promotes myeloid bias of *Tet2*-KO CMPs and deletion of *Tet2* within HSPCs is necessary for their expansion and myeloid bias. (a) WT and *Tet2*-KO mice were treated with IL1β or vehicle for five weeks (Fig. 1a) analyzed by flow cytometry and percentage of live $CD45^+$ cells which are CMPs, GMPs, and MEPs in the BM and spleen. **(b)** Lineage depleted BM cells were harvested from WT CD45.1 and *LysM-Cre Tet2*$^{-/-}$ CD45.2 (*LysM-Cre Tet2*-KO) mice into lethally irradiated wild-type $CD45.1^+CD45.2^+$ mice subsequently treated with IL1β or vehicle. The percentage of WT CD45.1 and *LysM-Cre Tet2*-KO CD45.2 cells out of all $CD45^+$ cells (chimerism) and the percentage WT CD45.1 and *Tet2*-KO CD45.2 cells which are myeloid in the PB. Error bars represent mean ± SEM. Student's two tailed t-Test was used to determine significance: *$p < 0.05$, **$p < 0.01$, ***$p < 0.001$, ****$p < 0.0001$.

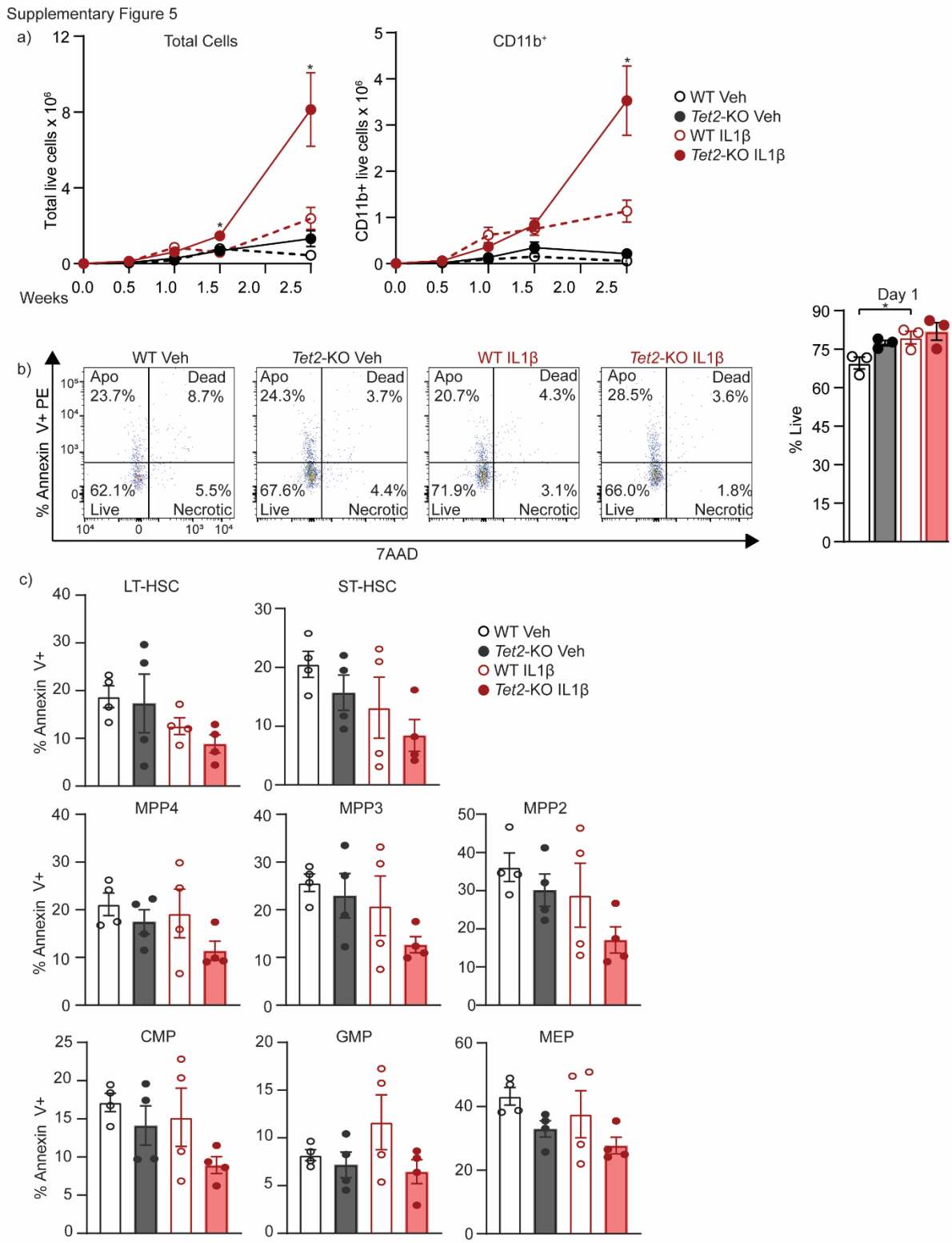

Supplementary Figure 5: IL1β-mediated expansion of *Tet2*-KO HSPCs is not associated with significant differences in the frequency of apoptosis or cell death. (a-b) *In vitro* competition of CD45.1 WT and CD45.2 *Tet2*-KO LSKs derived from BM and treated with or without IL1β (Fig. 3a); **(a)** number of total and myeloid cells overtime as quantified by flow cytometry **(b)** and percentage of live, apoptotic (Apo), dead and necrotic cells (n = 3 biological replicates) after 24 hours of culturing. **(c)** WT and *Tet2*-KO mice were treated with IL1β for four weeks (n = 4 mice/group) as described in Fig. 3b. The percentage of apoptotic ($7AAD^{-}Ann\ V^{+}$) cells for HSPC subsets was quantified by flow cytometry. Error bars represent mean ± SEM. Student's two tailed t-Test was used to determine significance: *$p < 0.05$, **$p < 0.01$, ***$p < 0.001$, ****$p < 0.0001$.

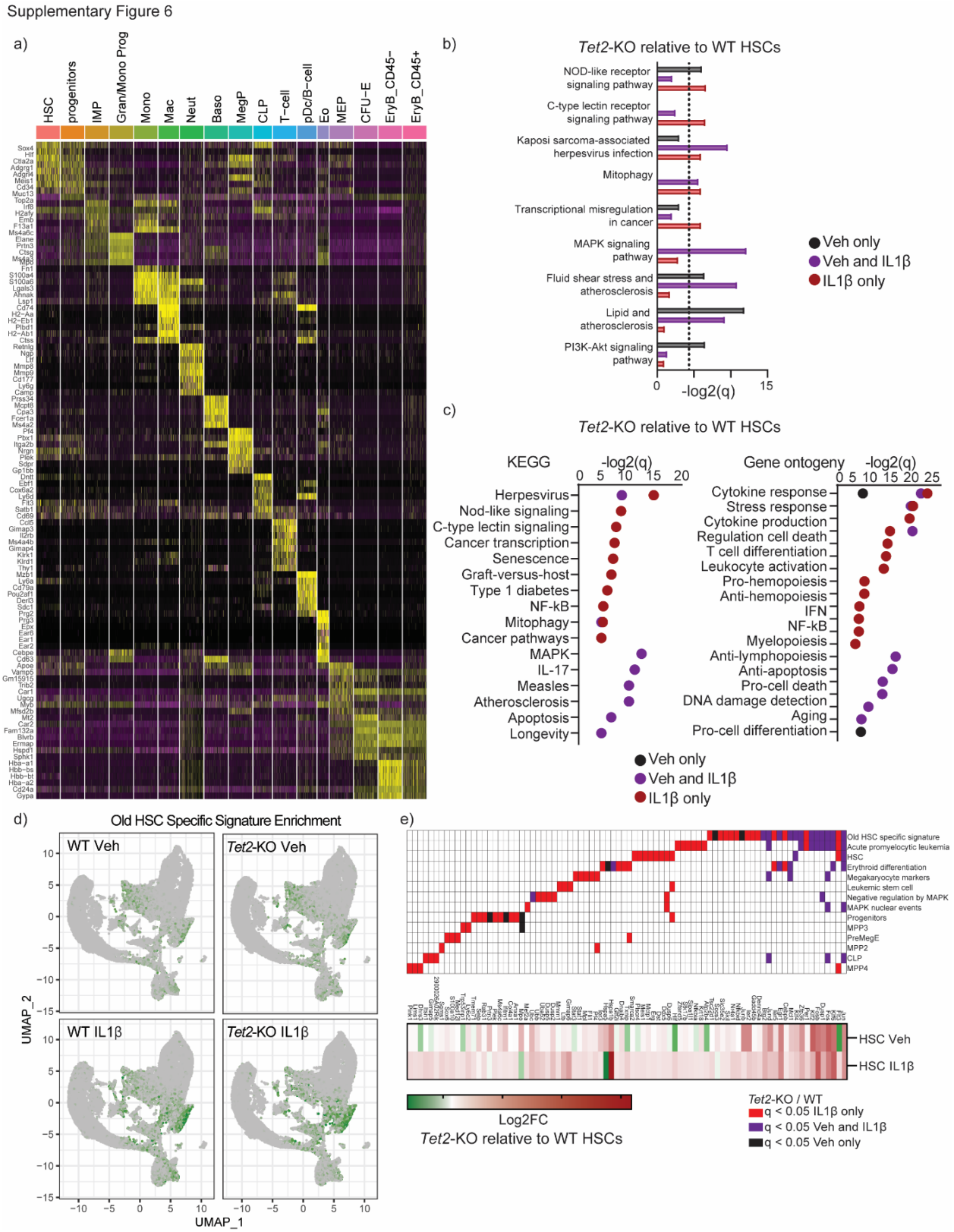

Supplementary Figure 6: 10x single cell RNA sequencing to identify cellular clusters from *Tet2*-KO and WT mice with and without IL1β stimulation *in vivo*. (a) Heatmap showing gene expression of cluster defining genes for individual cells from each cluster. **(b)** EnrichR ontology (KEGG 2021 human) of DEGs upregulated in *Tet2*-KO relative to WT HSCs in vehicle alone (black), IL1β alone (red) or in both (purple) with q values calculated by EnrichR. **(c)** STRING KEGG response to cytokine from biological process gene ontology (GO:0034097) and MAPK signaling pathway from KEGG Pathways (mmu04010) of DEGs upregulated in *Tet2*-KO relative to WT only under vehicle alone (black), IL1β alone (red), or both conditions (purple) with q values calculated by STRING. **(d)** Enrichment of transcriptional signature specific to old

HSCs[21]. **(e)** Heatmap of upregulated DEGs in *Tet2*-KO relative to WT HSCs with and without IL1β stimulation. Genes are the lead genes for enriched pathways by GSEA analysis (top panel), with squares representing significance when treated with IL1β only (red), vehicle only (black) or both (purple), with log fold change in gene expression (bottom panel) and q values calculated by EnrichR.

Supplementary Figure 7

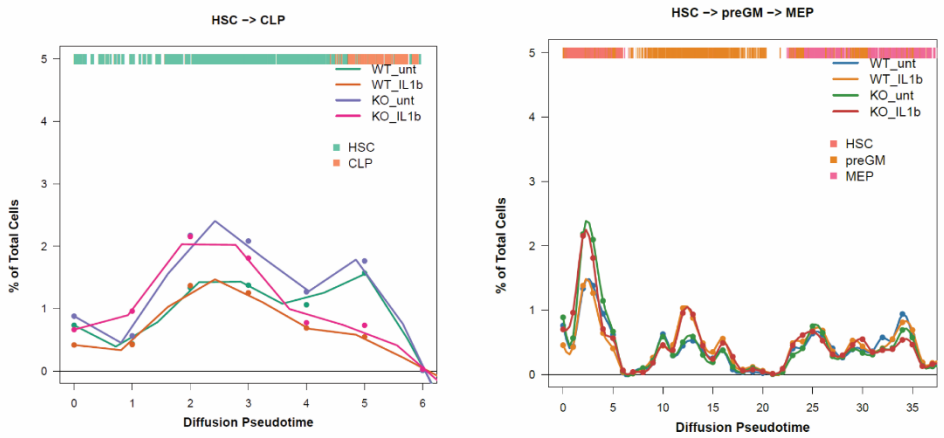

Supplementary Figure 7: Diffusion pseudotime analysis reveals *Tet2*-KO undergoes normal lymphoid and erythroid lineage commitment. Diffusion pseudotime from scRNAseq for indicated lineages (Fig. 4).

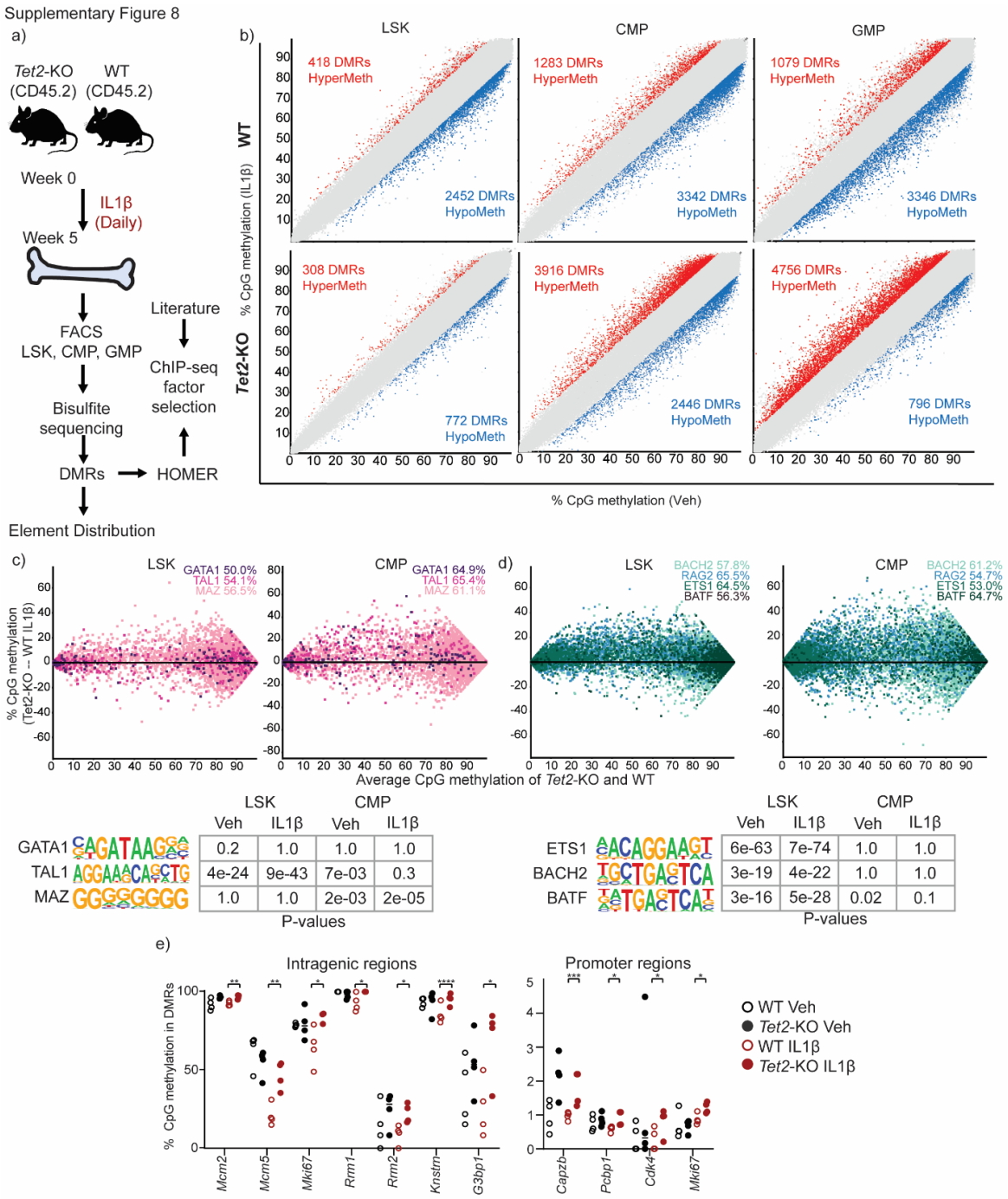

Supplementary Figure 8: *Tet2*-KO HSPCs resist IL1β driven methylation reduction of lineage specific enhancer regions and transcription factor binding sites. WT and *Tet2*-KO mice were treated for 4 weeks with or without IL1β (Fig. 4a), purified BM derived LSK, CMP, and GMP cells were analyzed by whole genome bisulfite sequencing (n = 4 mice/group). **(a)** Experimental design, **(b)** differentially methylated regions (DMRs) from 50 CpGs tiling of the whole genome (>10% methylation difference, q < 0.05, as determined by SeqMonk) between vehicle or IL1β treatment in WT or *Tet2*-KO cells. **(c)** Top, MA plots showing methylation difference for LSK and CMP cells derived from *Tet2*-KO and WT mice treated with IL1β using literature derived ChIP-seq binding sites of erythroid/megakaryocytic lineage specifying transcription factors (TFs). The percentage of sites with higher methylation in *Tet2*-KO than WT are shown in the top right corner of each graph. Bottom, significance of motif enrichment using HOMER analysis tool within DMRs for TFs. With q values calculated by Homer. **(d)** As in Supplementary Fig. 8c, but showing lymphoid lineage specifying TFs. **(e)** Selected examples of genes showing methylation differences within promotor (top) or intragenic (bottom) regions. Student's two tailed t-Test was used to determine significance except where otherwise specified in the figure legend: *p < 0.05, **p < 0.01, ***p < 0.001, ****p < 0.0001.

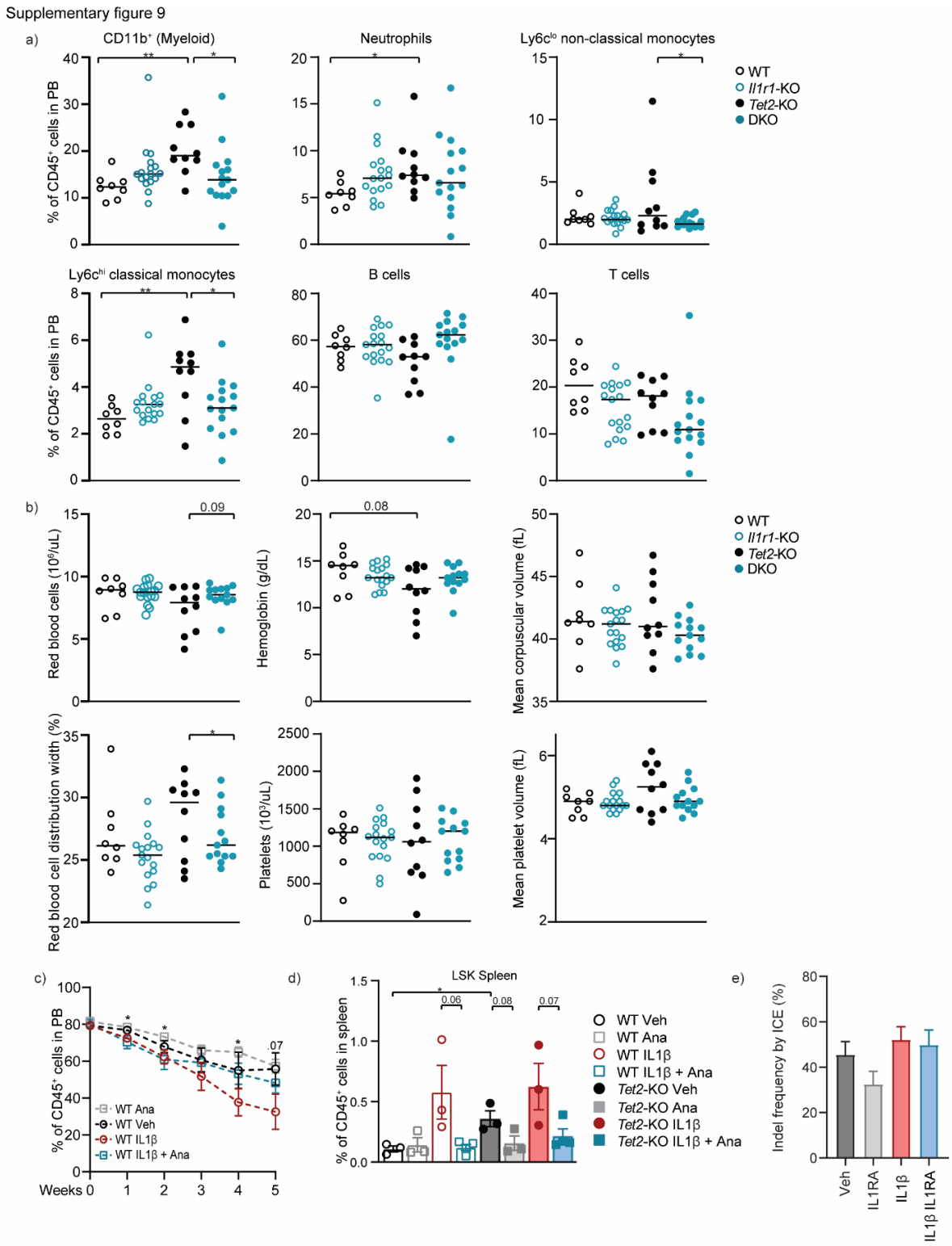

Supplementary Figure 9: Disrupting IL-1 signaling reduces granulocytic and monocytic expansion. Flow cytometry and differential blood cell count analyses of the PB of WT, *Tet2*-KO, *Il1r1*-KO, and DKO mice between 20 – 60 weeks of age (Fig. 6a). **(a)** Percentage of myeloid, neutrophils, ly6c^{lo} monocytes, ly6c^{hi} monocytes, B cells, and T cells in PB by flow cytometry and **(b)** differential blood cell counts showing red blood cell, hemoglobin, and platelet concentration, as well as mean corpuscular volume, red blood cell distribution width, and mean platelet volume. **(c)** percentage of WT CD45.1 donor cells out of all CD45^{+} cells (chimerism) in PB from experiment shown in Figure 6d-e, **(d)** percentage of LSK cells out of all WT CD45.1 and *Tet2*-KO CD45.2 donor cells in spleen with and without anakinra treatment in the presence and absence of IL1β. **(e)** Indel frequency of individually picked colonies Vehicle, IL1RA, IL1β and IL1β with IL1RA as determined by inference of CRISPR edits (ICE) Error bars represent mean ± SEM. Student's two tailed t-Test was used to determine significance: *$p < 0.05$, **$p < 0.01$, ***$p < 0.001$, ****$p < 0.0001$.